Sunniva Bjelland

Impact of Location of Frequency Reserves

Master's thesis in Energy and Environmental Engineering
Supervisor: Kjetil Uhlen
February 2019

Master's thesis

NTNU
Norwegian University of Science and Technology
Faculty of Information Technology and Electrical Engineering
Department of Electric Power Engineering

NTNU
Norwegian University of
Science and Technology

Sunniva Bjelland

Impact of Location of Frequency Reserves

Master's thesis in Energy and Environmental Engineering
Supervisor: Kjetil Uhlen
February 2019

Norwegian University of Science and Technology
Faculty of Information Technology and Electrical Engineering
Department of Electric Power Engineering

Acknowledgement

Working on this thesis has been very interesting, and I would like to thank my supervisor Professor Kjetil Uhlen for proposing the topic and for great guidance throughout the work with this thesis. His availability and feedback during the semester have been highly appreciated.

I would also like to thank Nicholas Stangeland and Aurora Flataker for proofreading and for constructive feedback.

And lastly, I would like to thank friends and family for all love and support.

Summary

The share of variable renewable production and HVDC interconnectors in the power system is increasing. This causes challenges in system operation thought large and frequent power fluctuations, reduced inertia and limited balancing reserves available from hydro generators. Active power regulation of synchronous generators operating in the system has traditionally been sufficient for maintaining the power balance. Reserve provision from other resources such as HVDC connectors, demand response and wind power plants are becoming increasingly important for the power balance. These resources may also provide reserves which are activated faster than the traditional reserves. The power output from these reserves are controlled based on local frequencies, which may vary significantly during disturbances. Location of the reserves will therefore impact performance of the reserves and system stability.

The goal of this thesis is to get further insight into how location of frequency reserves impacts system stability and frequency response. To assess the impact of location of frequency reserves, an aggregated model of the Nordic synchronous named Nordic 44, was simulated in PSS\E, and the response of frequency reserves were resembled through the use of a battery model. A 1200 MW fault was simulated through the outage of a generator, and all reserves were located at one location. Different fault locations and reserve locations were compared, and the results showed that fault location had a significant impact on the importance of location. For a fault in electrically remote locations, large initial power swings caused the initial power output from the reserves to increase when the reserves were placed close to the fault. At other locations, the initial impact of location were less significant. For all fault locations, the initial power output from the reserves were largest when reserves were placed close to the fault. The location did however have little impact on the frequency nadir. A benefit related to location of reserves was increased damping of low frequency oscillations when reserves were located at certain locations.

Sammendrag

Andelen av fornybar produksjon og kapasitet på HVDC kabler i kraftsystemet er økende. Det forårsaker store og hyppige variasjoner i kraftflyt, redusert kinetisk energi i systemet og begrensede reserver tilgjengelig fra vannkraftgeneratorer. Regulering av aktiv effekt fra vannkraftgeneratorer har tradisjonelt vært tilstrekkelig for å balansere ubalanser i kraftsystemet. Effektreserver fra andre ressurser slik som HVDC-kabler, lastrespons og vindkraftverk blir mer og mer viktig for å opprettholde kraftbalansen. Disse ressursene har også mulighet til hurtig effektregulering, og reserver kan derfor bli aktivert raskere enn for tradisjonelle reserver. Aktivering av reserver er basert på målinger av frekvensavvik. Frekvensavviket på ulike steder i systemet varierer ulikt som følge av en feil, og forskjellen i frekvens ved ulike lokasjoner kan være betydelige. Plasseringen til reserver vil derfor påvirke levert effekt fra reservene, og dermed også stabiliteten til systemet. En forenklet modell av det nordiske kraftsystemet ble brukt til å finne ut hvordan lokasjon påvirker aktivering av reserver og responsen til systemet. En batterimodell ble brukt til å etterligne responsen til reservene. Resultater fra simuleringene viser at i visse områder vil en feil føre til store lokale svingninger, og plassering av reserver i disse områdene vil derfor føre til aktivering av mer reserver rett etter at feilen skjer, sammenlignet med steder lenger vekk fra feilen. For andre feillokasjoner hadde plasseringen til reservene mindre betydning. For alle feillokasjoner hadde reserver som var plassert nær feilen størst aktivert rett etter at feilen var skjedd. Lokasjonen til reservene hadde likevel minimal innvirkning på maksimalt frekvensavvik. En positiv innvirkning relatert til lokasjon av reserver viste seg å være økt demping av svingninger i systemet for visse lokasjoner.

Table of Contents

List of Tables

List of Figures

Abbreviations

AVR	Automatic Voltage Regulator
API	Application Programming Interface
vRES	variable Renewable Energy Sources
FCR-N	Frequency Containment Reserves for Normal operation
FCR-D	Frequency Containment Reserves for Disturbances
ROCOF	Rate of Change of Frequency
TSO	Transmission System Operator

Chapter 1

Introduction

1.1 Background and Objective

The frequency of the power system is determined by the power balance in the system. Deviations between planned and real time power demand, or sudden outages of generators will cause power unbalances in the system. To mitigate large frequency excursions due to power imbalance, frequency reserves are of vital importance. When deviations from the nominal frequency occur, primary frequency resources are automatically activated and restores the frequency to an acceptable value.

However, following a disturbance, not all locations will be affected similarly. Locations close to the fault is typically more severely affected than locations far from the fault. Power output from primary frequency reserves are based on local frequency deviations, and reserves located close to the fault are therefore likely to be released at an earlier instance as compared to reserves located further away. Location of reserves will therefore have an impact on system stability.

In the Nordic system, primary frequency control have mostly been covered by hydro and thermal generators. In scenarios with high share of HVDC import and vRES production, available reserves from synchronous generators may be limited. Reserve provision based on asynchronous resources such as HVDC, wind power and demand response is therefore necessary on the balancing market.

With a high share of asynchronous production, low system inertia may cause a higher rate of change of frequency during disturbances. Fast activation of reserves may then be necessary for stable system operation. New balancing products with faster activation time than the traditional primary reserves are therefore introduced by TSOs in order to increase stability margins.

The growing share of vRES and HVDC connections has caused a need for flexibility and new technologies on the balancing market. More cooperation between TSOs on the balancing market is believed to benefit system operation. Market based solutions are thereby

increasingly impacting the location of power reserves. It is therefore important to asses how the location of frequency reserves impacts the system response following a disturbance. Additionally, if new balancing products for fast frequency reserve activation are used to increase stability margins, the impact of location may be critical. The latency introduced by the fault propagation may cause a delay in activation of the reserves, and the benefit of fast response may therefore be reduced. Assessing the impact of location will therefore highlight benefits and drawbacks resulting from the locations of power reserves. Further insights on the impact of location will also provide a better foundation for determining and prioritizing which bids for frequency reserves to accept.

1.2 Scope

The goal of this thesis is to investigate how location and distance to the fault impacts power output from asynchronous frequency reserves whose power output depend on local frequency measurement. The main focus is to find out how distance to the fault will impact the effect of fast frequency reserves and system response.

1.3 Methodology

The impact of location of fast frequency reserves were analyzed PSS\E by using an aggregated model of the Nordic synchronous system. Primary frequency reserve activation from generator droop control was reduced, and the impact of locating all reserves in one area was analyzed and compared for different locations. The main focus of the simulations was the response from asynchronous frequency reserves with fast activation time. A battery model with short activation time was therefore used to represent the response from asynchronous resources. Simulations were conducted through the PSS\E Python API.

1.4 Outline

Background on current state and developments in the Nordic system which serves as a motivation for the studies presented in this thesis is provided in section 2.1. Chapter 2 continues with fundamental background theory on how generators and the system is affected by active power disturbances. Factors influencing fault propagation in a larger system is discussed in section 2.5. During the simulations, it was observed that the location of reserves had a significant impact on the damping and oscillatory stability of the system. Background theory on oscillatory stability is therefore included in chapter 2.

Chapter 3 describes the model used, modification and assumptions made. In chapter 4, simulations and results are presented. Further discussion of the results are given in chapter 5. In chapter 6, conclusions and future work are presented.

Chapter 2

Background and theory

2.1 Frequency regulation in the Nordic system

The Nordic synchronous system comprises the power system of Sweden, Norway, Finland and Eastern Denmark. The system is divided into 11 elspot areas corresponding to the main bottlenecks in the grid [18]. The Nordic elspot areas are shown in Figure 2.1.

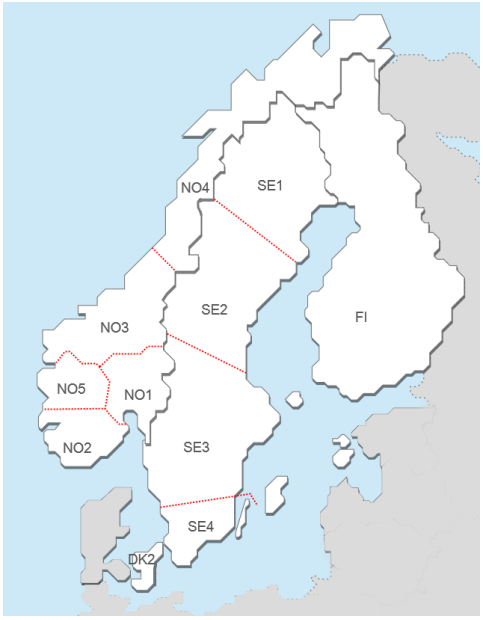

Figure 2.1: Elspot areas of the Nordic synchronous system. Modified from figure in [30]

Primary frequency reserves in the Nordic system are named Frequency containment Resources (FCR), and two types of FCR products exists:

- FCR-N

  - FCR for normal operation. Used for stochastic fluctuations in the power balance. Activated in the frequency range 49.9 – 50.1 Hz [18]
- FCR-D

  - FCR for disturbances. Used for large disturbances such as generator outages. Activated in the frequency range 49.9 – 49.5 Hz [18]

FCR-N is a symmetric product and the FCR-N provider must be able to regulated the agreed capacity both upwards and downwards. FCR-D reserves are currently only procured for upwards regulation [29].

2.1.1 Current reserve requirements

The total reserve requirement for FCR-N is set based on annual consumption, and is currently set to 600 MW, giving a total system response of 6000 MW/Hz [18]. The total FCR-D requirements are set based on the dimensioning incident, and an example of distribution of FCR-D requirements for the Nordic TSOs are shown in Table 2.1. Since the dimensioning incident is determined by the operating state of the system, requirements for FCR-D reserves are currently calculated on a weekly basis, or more often if needed [9].

Country	**Dimensioning incident [MW]**	**FCR-D reserve [MW]**
Denmark	600	176.5
Finland	880	258.8
Norway	1200	352.9
Sweden	1400	411.8
	Total	**1200**

Table 2.1: FCR requirements for the Nordic TSOs [6]

2.1.2 Future impacts on frequency quality

As the normal frequency range is set to $\pm$100 mHz, it is assumed that a disturbance is occurring when the frequency is outside the normal operating range [23]. The number of minutes outside of the normal band (MoNB) is often used as an indication on frequency quality, and the Nordic TSOs reports a trend with increasing MoNB [31, 23]. However, according to [23], over 90% of the MoNB was caused by normal power fluctuations, and not by disturbances. Since FCR-D are activated for frequency deviation larger than $\pm$ 100 mHz, FCR-D will be activated during normal operation, and less FCR-D reserves will be available in case of a disturbance.

The main reasons for increasing MoNB is related to increasing share of production from vRES in addition to large and frequent variations on HVDC power flows [31]. Low frequency oscillations in the system are also reported to have significant influence on the frequency quality [23, 10]. Analysis performed in [10] showed that MoNB reduces with around 40% when low frequency oscillations were excluded. The impact of low frequency

oscillations on MoNB do however seem to be stable over years [10].

In the years towards 2025, the Nordic TSOs are expecting power imbalances to increase [31]. Several HVDC connections are being build, causing an increase in the capacity to other synchronous systems. In case of high HVDC import, the kinetic energy in the system will reduce. A high export case will also impact the frequency regulation through additional requirements for FCR-D downwards reserves [29]. An increasing share of vRES in the Nordic system is also likely to contribute in more frequent power fluctuations. The impact of vRES is partly due to the fluctuating nature of vRES and partly due to reduced system inertia making the system frequency more sensitive to power fluctuations.

2.1.3 Fast Frequency Resources

As increasing power fluctuations challenges frequency stability, some TSOs are considering additional products for fast frequency response (FFR). FFR are frequency reserves with faster activation time than FCR. Typical candidates for FFR provision are flexible loads, battery storage systems, HVDC connections, or renewable resources operating below their maximum power output (deloaded mode). Such asynchronous resources may provide fast and accurate power regulation, either through power electronics or through fast regulation of power demand.

In systems with high share of vRES, FFR is already a part of the balancing market. In Ireland, the introduction of FFR and other new balancing products has contributed to making the Irish power system able to allow a vRES share of up to 60%. The Irish system operator aims at a 75% vRES limit by 2020 [14, 5]. The TSO of Great Britain, National Grid, has launched a FFR-service called "Enhanced Frequency Response", and fully contracted reserves must be delivered within 1 second [26]. In 2018, the Norwegian TSO, Statnett, conducted a pilot project on FFR where contracted reserves were activated within 2 seconds [29]. The Nordic TSOs are currently considering introduction of the FFR product on the ancillary market, and a market release is anticipated in 2020 [29].

2.1.4 Balancing market

Activation of frequency reserves requires available transmission capacity. Bottlenecks in the grid may therefore prevent the cheapest bids from being activated. In some cases, it may be socio-economic beneficial to reserve additional transmission capacity for activation of primary reserves [9]. Reserving additional transmission capacity for primary reserves will however affect prices in the spot market.

The Norwegian TSO, Statnett, currently procures most of their FCR-D reserves through a mandatory droop requirement for all generating units larger than 10 MW [29]. The mandatory droop requirement provides little control of location of the reserves, and Statnett is planning on removing this requirement [29]. It is assumed that removing the mandatory droop requirement will provide incentives to the market participants in the areas were reserves are needed the most.

Due to the increasing share of vRES, the Nordic TSOs sees an increasing need for flexibility in the balancing markets [31]. Flexibility from hydro power is limited, and may also become more expensive due to increasing competition from continental Europe [31]. Balancing services provided from other resources may therefore contribute to a more cost efficient use of balancing reserves and transmission capacity.

To facilitate an efficient use of resources and a broader technology mix in the balancing market, ENTSO-E (the European Network of Transmission System Operators for Electricity) is encouraging closer cooperation among TSOs and harmonization of requirements for balancing products [8]. New requirements on integration of balancing services has led to several projects on integration of the balancing markets [7]. These projects focuses on common market platforms for secondary reserves, and the Nordic TSOs will join these markets when the platforms are launched [32].

The balancing market for FCR is not yet integrated, but cooperation is considered beneficial. The Austrian, Belgian, Dutch, French, German and Swiss TSOs have started a project with a common merit order list for FCR [8]. In the Nordic, TSOs may trade FCR with each other [29]. Trade is however limited as 2/3 of the contracted reserves must be within the TSOs control area [9]. Bottlenecks in the grid may also restrict trade between TSOs [29].

2.2 Impact of location of power reserves

The changes in the market structure is beneficial to the system operation by enabling more flexible and intentional placement of the power reserves. Faster response from new FCR and FFR providers is also assumed to contribute in enhancing the frequency quality. Activation of FCR and FFR reserves is based on local frequency measurements. Local frequencies may however vary depending on the fault locations and it is therefore likely that the reserve location will have an impact on the reserve power output. The benefit of fast response from FFR may be lost if the frequency at the FFR location is insensitive to the disturbance. Additionally, for the TSOs to introduce proper incentives on the balancing markets, and also to take advantage of the increased flexibility when locating reserves, it is of interest to asses the impact of location of power reserves on the dynamic response of the system.

2.3 Frequency stability and control

The electrical frequency in a synchronous system is determined by the rotor speed of the generators operating in the system. In the Nordic synchronous system, the nominal system frequency is set to 50 Hz, and to maintain constant frequency, constant rotor speed is required. The rotor speed can be described using Newtons second law for rotating masses and from this relation, the swing equation describing the system frequency can be derived.

Parts of section 2.3.1 and section 2.3.2 are redrafts from [2]

2.3.1 The swing equation

When friction and windage losses of the machine are neglected, the rotor speed can be expressed through newtons second law as [22]

$$J\frac{d\omega_m}{dt} = \tau_{mech} - \tau_{el} \tag{2.1}$$

where ω_m is the angular velocity of the rotor [rad/sec], τ_{mech} is the mechanical torque applied to the rotor shaft [Nm], τ_{el} is the electrical torque [Nm], and J is the combined inertia of the turbine and the rotor [Kg m^2].

(2.1) may be expressed in per unit by defining the per unit power and speed base values as S_N and ω_s, where S_N is the rated apparent power of the machine and ω_s is the synchronous speed. Expressing ω_m, J, τ_{el} and τ_{mech} as their per unit values times their respectively base values yields:

$$\omega_m = \omega_s\omega \qquad J = \frac{2HS_N}{\omega_s^2} \qquad \tau_{mech} = \frac{S_N}{\omega_s}\tau_m \qquad \tau_{el} = \frac{S_N}{\omega_s}\tau_e \tag{2.2}$$

where H is the normalized per unit inertia constant given in seconds, ω is the per unit rotor speed, τ_{mech} is the per unit mechanical torque and τ_{el} is the per unit electrical torque. Inserting the expressions in (2.2) into (2.1) yields

$$\frac{2H}{\omega_s}\frac{d}{dt}\Delta\omega_s\omega = \tau_m - \tau_e \tag{2.3}$$

The rotor position can be referred to with respect to the synchronous reference frame, and the rotor velocity can thus be expressed as [22]

$$\omega_m = \omega_s + \Delta\omega_m = \omega_s + \frac{d\delta_m}{dt} \tag{2.4}$$

Where δ_m is the mechanical rotor angle with respect to the synchronous reference frame. $\Delta\omega_m = \frac{d\delta_m}{dt}$ represents the rotor speed deviation in mechanical radians per second [22]. On per unit form, the speed deviation becomes

$$\Delta\omega = \frac{\Delta\omega_m}{\omega_s} = \frac{1}{\omega_s}\frac{d\delta_m}{dt} \tag{2.5}$$

Inserting (2.5) into (2.3) gives

$$\frac{2H}{\omega_s}\frac{d^2\delta_m}{dt^2} = \tau_m - \tau_e \tag{2.6}$$

When considering small changes around $\omega = 1$, the approximation $P \approx \tau$ may be used, and (2.6) can be written as

$$2H\frac{d\omega}{dt} = P_m - P_e \tag{2.7}$$

An additional term $P_D = D\Delta\omega$ is often included in the swing equation such that (2.7) can be written as

$$2H\frac{d\omega}{dt} = P_m - P_e - P_D \tag{2.8}$$

In (2.7) P_D account for damping effects in the system. Such damping effects may be due to frequency dependency of loads [20] or due to the effects of generator damper windings [22].

2.3.2 Frequency dynamics

Following a sudden power deficit, the dynamic response of the system can be described in four stages [22]:

- Stage I - Rotor Swings
- Stage II - Frequency drop
- Stage III - Primary frequency control
- Stage IV - Secondary frequency control

The system frequency response during stage II, stage III and stage IV is illustrated in Figure 2.2

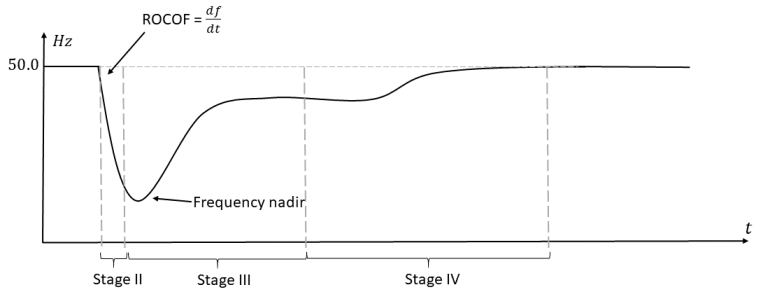

Figure 2.2: System response during a power deficit

Stage I - Rotor Swings

A sudden change in the active power balance of a generator will cause an initial displacement of the generator rotor angle. The active power balance of the generator is not in equilibrium, and due to rotor inertia, the rotor will oscillate before it settles at equilibrium. A simplified analysis of the rotor swings can be performed by considering a generator represented by its transient emf, E', and its transient equivalent reactance X'_d operating against an infinite bus with voltage V_s and network reactance X. The single machine infinite bus system can be seen in Figure 2.3, and the power angle characteristics of the machine is given by

$$P_e = \frac{E'V_s}{X'_d + X} \sin(\delta') \tag{2.9}$$

A sudden change in the electrical power output will shift the power characteristics of the generator upwards. Due to rotor inertia, the rotor cannot change instantaneously. The generator will therefore operate in point 2 immediately following the fault. At this point, the electrical power output is larger than the mechanical power input, and the rotor will

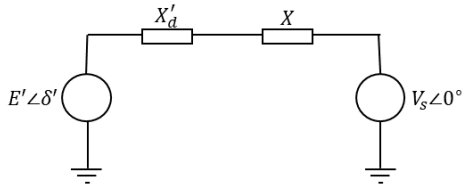

Figure 2.3: Generator operating against infinite bus

start decelerating towards the new equilibrium in point 4. Due to rotor inertia, the rotor will continue beyond point 4 to point 3. Since mechanical power in point 3 is larger than the electrical power in point 3, the rotor will swing back again towards point 2. The rotor will continue to oscillate, and due to damping effects in the system, it will stabilize at the equilibrium in point 4.

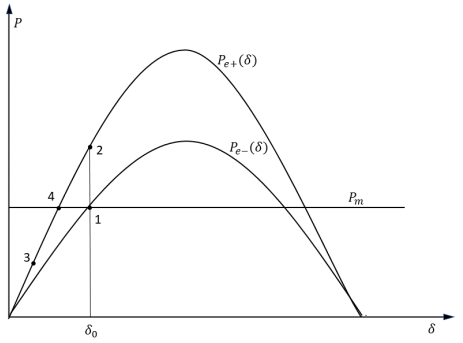

Figure 2.4: Rotor swings in remaining generator due to sudden outage of parallel connected generator. Based on figure in [22]

Stage II - Frequency drop

In stage II, the frequency starts to drop. To regain power balance, kinetic energy from the generators is released, and the rotor speed reduces. The rate of change of frequency at each generator will depend on the power imbalance at the generator and its inertia constant. However, if all generators remain in synchronism, the speed deviation is approximately similar for all generators [22]. The speed deviation may therefore be written as

$$\frac{\Delta\omega_1}{dt} \approx \frac{\Delta\omega_2}{dt} \approx ... \approx \frac{\Delta\omega_n}{dt} \approx \epsilon \tag{2.10}$$

From the swing equation, as formulated in (2.8) the speed deviation can be expressed as $\frac{d\omega}{dt} = \frac{\omega_s \Delta P}{2HS_N}$. By replacing the expression for $\Delta\omega$ into (2.10), the frequency deviation of the i'th generator can be expressed as

$$\frac{\Delta P_1 \omega_s}{2HS_{N_1}} \approx \frac{\Delta P_2 \omega_s}{2HS_{N_2}} \approx ... \approx \epsilon \tag{2.11}$$

From (2.11), the change in power of the i'th generator can be expressed as

$$\Delta P_i = \epsilon \frac{2H_i S_{N_i}}{\omega_s} \tag{2.12}$$

If P_T is the total power increase from the generators, the total system response can be expressed as

$$\Delta P_T = \sum_{i=1}^{n} \Delta P_i = \epsilon \sum_{i=1}^{n} \frac{2H_i S_{N_i}}{\omega_s} \tag{2.13}$$

Rearranging (2.13) gives the power taken by each generator in the system as

$$\Delta P_i = \frac{H_i S_{N_i}}{\sum_{k=1}^{n} H_k S_{N_k}} \Delta P_T \tag{2.14}$$

The term $H_i S_{N_i}$ represent the kinetic energy of the generator, and as can be seen from (2.13) , the power taken by each generator depends on the generators kinetic energy in proportion to the total kinetic energy in the system.

Stage III - Primary frequency control

The primary frequency control aims at stabilizing the system frequency to an acceptable level, and is typically performed through the governor droop control of the generators. The droop coefficient, ρ_i, represents the increase as a percentage of the machine power rating, P_{Ni}. The governor droop control will increase the mechanical power output proportional to the frequency deviation. The change in mechanical power from the i'th generator may therefore be written as

$$\Delta P_{m_i} = \frac{P_{N_i}}{\rho_i} \frac{\Delta \omega_s}{\omega_s} \tag{2.15}$$

The total change in production from the generators equals the sum of change in power output from each generator. After primary frequency control has been activated, the total change in mechanical power output can be expressed as [22]

$$\Delta P_{m,tot} = \sum_{i=1}^{n} \Delta P_{mi} = \frac{\Delta f}{f_s} \sum_{i=1}^{n} \frac{1}{\rho_i} P_{Ni} \tag{2.16}$$

The combined droop characteristics of all generators in the system gives the system frequency response to a power change. Figure 2.5, illustrates effect of combined droop response from two generators. The total system frequency response may therefore be written as

$$K_T = \sum_{i=1}^{n} K_i \tag{2.17}$$

Where K_i is defined as

$$K_i = \frac{\Delta P_{mi}}{\Delta f} = \frac{P_N}{\rho f_s} \tag{2.18}$$

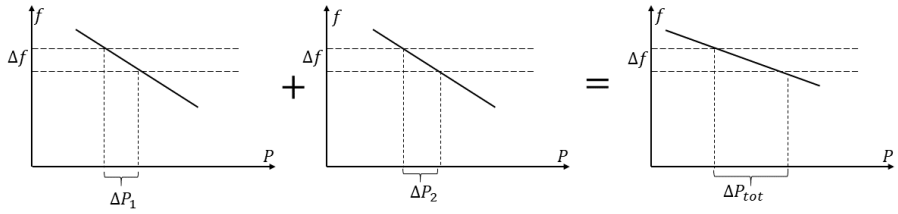

Figure 2.5: The combined droop characteristics of two generators. Based on figure in [20]

Stage IV - Secondary frequency control

As can be seen from Figure 2.5, the new steady state frequency after the power increase will be lower than the original operating frequency. To regain nominal system frequency, secondary frequency reserves are activated. The secondary frequency control is a centralized control mechanism where power reference set-points of the generators are changed. The droop characteristics are thereby shifted upwards as illustrated by the dashed line in in Figure 2.6. If the generators are operating in point 2 after primary frequency control, there will be a steady state frequency deviation defined by $f_1 - f_2$. By shifting the power characteristics upwards, the system will operate in point 3, and the nominal system frequency is regained. Secondary reserves will eventually be replaced by tertiary reserves.

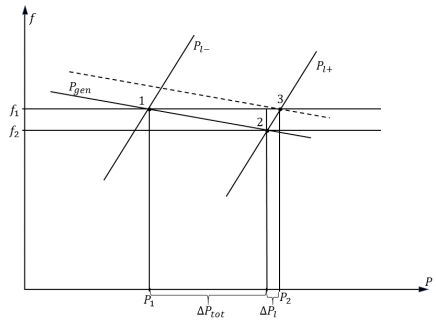

Figure 2.6: Pre- and post disturbance operating points [22]. After primary frequency control, the new operating point is given by point 2. Secondary frequency control shifts the operating point upwards to point 3.

2.4 Frequency control with FFR

The impact of adding FFR to the frequency control is shown in Figure 2.7. It can be seen that the FFR acts during the frequency drop, causing less drop in frequency. Primary fre-

quency reserves are typically fully activated within 30 seconds. This allows for a relatively long duration of the frequency drop in stage II. In cases with low system inertia, slow activation of primary frequency response might cause the frequency to reach critical values. Fast activation of FFR might therefore contribute in arresting the frequency nadir at an earlier instance as illustrated in Figure 2.7

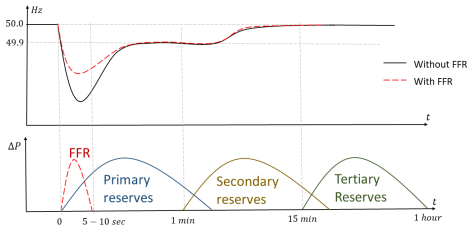

Figure 2.7: Power system frequency response to a power deficit. Adapted from [33]

2.5 The effect of electrical distance

In section 2.3.2, a generator connected to an infinite bus system was considered. During the initial swing, generators in the system will be affected differently. The difference in initial power swing of generators in the system will therefore contribute to differences in frequencies at different locations immediately following the fault. To analyze the impact of a disturbance somewhere in the system, a multi-machine system is considered with machines represented by a constant emf behind a transient reactance. The power flow representation of the system might be reduced to machine basis by including machine reactances in the network admittance matrix, and consider the machine terminal voltages [1]. Angular differences is then represented by the machine rotor angles. The power flow injected at machine i is given by [1]

$$P_{e_i} = \sum_{i=1}^{N} |Y_{ij}||E_i||E_j| \sin(\delta_{ij}) \tag{2.19}$$

Where E_i and E_j is the terminal voltages of the machines, $\delta_{ij} = \delta_i - \delta_j$ where δ_i and δ_j are the machine angles, and $|Y_{ij}|$ is given by the network admittance matrix. A small disturbance away from the initial operating point can be defined such that $\delta_{ij} = \delta_{ij0} + \Delta\delta_{ij}$, where δ_{ij0} is the initial difference in machine angles. For small values of $\Delta\delta_{ij}$, the approximation in (2.20) may be used [1].

$$\sin(\delta_{ij}) = \sin(\delta_{ij0})\cos(\Delta\delta_{ij}) + \cos(\delta_{ij0})\sin(\Delta\delta_{ij}) \approx \sin(\delta_{ij0}) + \Delta\delta_{ij}\cos(\delta_{ij0}) \tag{2.20}$$

The power taken by machine i due to the change $\Delta\delta_{ij}$ can be found by calculating the power output for $\delta_{ij} = \delta_{ij0} + \Delta\delta_{ij}$. By using the approximation in (2.20), the new power output is given by [1]

$$P_{e_i}(\delta_{ij0} + \Delta\delta) = \sum_{\substack{j=1 \\ j\neq i}}^{n} |Y_{ij}||E_i||E_j|[\cos(\delta_{ij0}) - \Delta\delta_{ij}\sin(\delta_{ij0})] \tag{2.21}$$

Since the term δ_{ij0} is constant, the change in power is due to the term $\Delta\delta_{ij}$, and the incremental change in power due to a incremental change $\Delta\delta_{ij}$ is given by [1]

$$\Delta P_{e_i} = -\sum_{\substack{j=1 \\ j\neq i}}^{n} |Y_{ij}||E_i||E_j| \sin(\delta_{ij0})\Delta\delta_{ij} = \sum_{\substack{j=1 \\ j\neq i}}^{n} P_{s_{ij}}\Delta\delta_{ij} \tag{2.22}$$

where $P_{s_{ij}} = |Y_{ij}||E_i||E_j| \sin(\delta_{ij0})$ is the synchronizing power coefficient between machine i and j. The synchronizing power coefficient reflects how much the power changes at machine i due to an angular change at machine j.

To better understand the effect of how the synchronizing power coefficient affects the immediate effect of a fault in the system, an example from [1] may be considered. The four bus system is shown in Figure 2.8, and at $t = 0$, there is a sudden increase in load at bus 4. The load increase causes a sudden increase in voltage angle at bus 4 given by $\Delta\delta_4$.

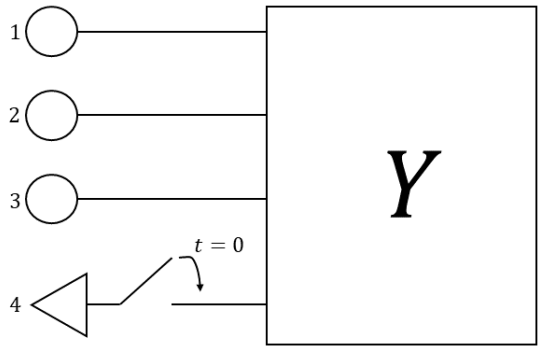

Figure 2.8: 4 bus system connected through a network given by the Y bus matrix. Based on figure in [1]

The rotor inertia of the generators will prevent any change in the rotor angle immediately following a fault, and at $t = 0^+$ we therefore have

$$\begin{aligned} \Delta\delta_{ij} &= 0 \\ \Delta\delta_{i4} &= \Delta\delta_i - \Delta\delta_4 = -\Delta\delta_4(0^+) \\ \Delta\delta_{4j} &= \Delta\delta_4 - \Delta\delta_j = \Delta\delta_4(0^+) \end{aligned} \tag{2.23}$$

By inserting (2.23) into (2.22). The power taken by each generator may be found as [1]

$$\Delta P_i(0^+) = -P_{si4}\Delta\delta_4(0^+) \tag{2.24}$$

And the power injected at node 4 is given by

$$\Delta P_4(0^+) = -\sum_{j=1}^{n} P_{s_{j4}}\Delta\delta_4(0^+) \tag{2.25}$$

By solving (2.25) for $\Delta\delta_4(0^+)$ and inserting into (2.24) , the power taken by each generator can be expressed as a function of its synchronizing power coefficient between generator i and 4.

$$\Delta P_i(0^+) = \frac{P_{si4}}{\sum_{j=1}^{n} P_{sj4}} \Delta P_4(0^+) \tag{2.26}$$

As seen from (2.26), the initial power taken by a generator depends on the share of synchronizing power coefficient between the generator and the location and the total synchronizing power coefficient between the fault location and all other locations. From (2.22), it can be seen that the synchronizing power coefficient depends on system admittances, voltages and initial operating angles. If voltages are assumed constant and differences in angles are assumed small, the synchronizing power coefficient will mainly depend on system topology. Generators electrically close to the fault will therefore take a larger share of the load regardless of their size [1].

2.6 Fault propagation in the system

After the initial power swings, the fault will propagate in the system according to power flow and angular differences between buses. Inserting (2.19) into the swing equation as expressed in (2.7) gives equation (2.27) [1]

$$2H_i \frac{d\omega_i}{dt} = P_{mi} - \sum_{j=1}^{n} |Y_{ij}||E_i||E_j| \sin(\delta_i - \delta_j) \tag{2.27}$$

If the mechanical power P_{mi} and the voltages $|E_i|$ and $|E_j|$ are assumed constant, it can be seen from (2.27), that the change in frequency at the individual nodes will depend on changes in the angle at neighbouring nodes. It can also be seen that a high reactance (small admittance) between node i and j reduces the impact of changes in the relative angle between node i and j. If there is a power deficit at node j, the frequency at node j will therefore drop lower before frequency at node i is affected. The system impedance is therefore contributing to a latency in the fault propagation.

As seen from (2.27), when the system becomes large, fault propagation is a complex function of grid topology and local inertia. The impact of grid topology with various combinations of inertia distribution was analyzed in [34]. A non-meshed (string) and a meshed (triangle) topology was compared for a three bus system, and a large power outage was applied at one of the buses. The results presented in [34] showed that for a non-meshed configuration, large power and frequency oscillations occurred in the faulted area. The meshed configuration showed a significant improvement in damping the oscillations, but combinations of high inertia in the other areas caused the faulted area to loose synchronism.

Further studies on local rate of change of frequencies were performed in [4]. The results presented in [4] shows that synchronizing power coefficient and distribution of inertia will

affect local ROCOF, which is in accordance with the theory presented in section 2.5. Results in [4] also indicated that distribution of inertia had little effect on system ROCOF, as system ROCOF was defined as the weighted average of local ROCOFs.

2.7 Angular stability

The results which will be presented in chapter 4 shows that locations of frequency reserves has an impact on angular stability. Different angular responses to a disturbance is shown in Figure 2.9. The solid line represent stable response to a disturbance, whereas the dotted line and the dashed line represent first swing instability and oscillatory instability, respectively.

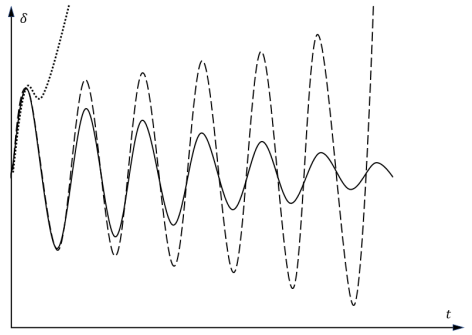

Figure 2.9: Types of angular stability. Based on figure in [20]

2.7.1 First swing stability

First swing instability occurs when the generator angle continues to increase after the first swing and looses synchronism with the rest of the system. First swing stability is related to the mechanisms of the first rotor swing following a disturbance, which was analyzed in section 2.3.2. The discussion in section 2.3.2 was however based on the assumption that the generator could be represented by a constant transient emf behind a reactance. Generators operating in power system usually have fast acting AVR which contributes in increasing the voltage, and thereby shifts the power-angle characteristics upwards. The first swing stability is thereby enhanced, and the generator may withstand larger rotor swings. It should however be noted that the AVR can only act as long as the field current limit is not reached [22].

2.7.2 Oscillatory stability

Oscillatory instability occurs when the amplitude of the rotor swings increases until the generator loses synchronism. In this case, the instability is not necessarily caused by the initial large disturbance, but rather that the post fault system condition is not stable

for small disturbances [20]. Small disturbances are usually defined as disturbances sufficiently small such that system linearization is valid [20].

The oscillatory behaviour of a generator can be analyzed by considering a generator connected to an infinite bus as shown in Figure 2.10.

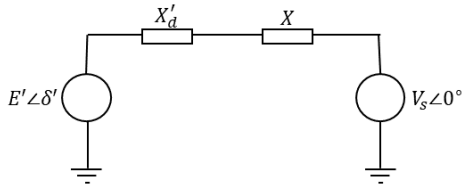

Figure 2.10: Synchronous machine connected to an infinite bus. Based on figure in [20]

From section 2.3.1, it is known that the rotor swings during a disturbance will follow the swing equation. The swing equation as given in (2.6) can be rearranged, and with damping effects included, it can be written as

$$\frac{d^2\delta}{dt^2} = \frac{\omega_s}{2H}(\tau_m - \tau_e - D\frac{d\delta}{dt}) \tag{2.28}$$

The active power produced by the machine can be written as

$$P_e = \frac{E'V_s \sin(\delta')}{X'_d + X} \tag{2.29}$$

By neglecting stator resistance, the terminal power becomes equal to the air gap power, and in per unit, the air-gap torque can be assumed equal to the air-gap power [20]. The electrical torque produced by the machine can therefore be written as

$$\tau_e = P = \frac{E'V_s}{X_T}\sin(\delta') \tag{2.30}$$

For small disturbances, the system equations can be linearized around an initial operating point defined by

$$\begin{aligned} \delta &= \delta_0 + \Delta\delta \\ \tau_e &= \tau_{e_0} + \Delta\tau_e \\ \tau_m &= \tau_{m_0} + \Delta\tau_m \end{aligned} \tag{2.31}$$

When linearizing, the electrical torque given in (2.30), the change in electrical torque can be expressed as [20].

$$\Delta\tau_e = \frac{\partial\tau_e}{\partial\delta}\Delta\delta = \frac{E'V_s}{X_T}\cos(\delta_0)\Delta\delta = K_s\Delta\delta \tag{2.32}$$

Inserting the expressions in 2.31 and 2.30 into equation 2.28 yields

$$\frac{d^2\Delta\delta}{dt^2} = \frac{\omega_s}{2H}(\Delta\tau_m - K_s\Delta\delta - D\frac{d\delta}{dt}) \tag{2.33}$$

Equation 2.28 is often called the linearized swing equation[21], and it is a second order differential equation with solution given by (2.34) [20]

$$\Delta\delta = \Delta\delta(0)e^{-\frac{Dt}{4H}}cos(\omega_n t - \beta) \tag{2.34}$$

The parameters ω_n and β in equation 2.34 are given by

$$\beta = atan\left(\frac{D}{4H\omega_n}\right) \tag{2.35}$$

$$\omega_n = \sqrt{\frac{K_s\omega_s}{2H} - \frac{D^2}{4H}} \tag{2.36}$$

The per unit damping power coefficient D usually small such that the natural frequency becomes [21]

$$\omega_n \approx \sqrt{\frac{K_s\omega_s}{2H}} \tag{2.37}$$

When analyzing oscillations in power systems, the damping ratio is usually of interest. The damping ratio is determined from the roots of the characteristic equation. When assuming no change in mechanical torque, equation 2.33 can also be written on the form [20]

$$s^2 + \frac{D}{2H}s + \frac{K_s\omega_0}{2H} = 0 \tag{2.38}$$

By comparing 2.38 with the general form of the characteristic equation expressed as [20]

$$s^2 + 2\zeta\omega_n s + \omega_n^2 = 0 \tag{2.39}$$

it can be seen that $\frac{D}{2H} = 2\zeta\omega_n$. The damping ratio ζ can therefore be written as

$$\zeta = \frac{D}{4H\omega_n} = \frac{D}{2\sqrt{K_s 2H\omega_0}} \tag{2.40}$$

From equation 2.40, it can be seen that increasing the damping torque coefficient D will increase the damping ratio. When the synchronizing torque coefficient K_s increases, the damping ratio decreases. Increasing the per unit inertia constant H will decrease both ζ and ω_n. [20]

When considering first swing stability, it was shown that AVR contributed in increasing the first swing stability limit. When considering oscillatory instability, the AVR might contribute in reducing the stability limit. This is because the AVR increases the voltage by increasing the field current. The changing field current causes variations in the field flux linkage. The torque created by the variation in field flux linkage, may have a component which is in opposing phase to the speed deviation [21]. The damping of the machine will therefore be reduced, and in critical cases, the net damping may become negative. Reduced damping due to AVR is typical for machines with high loading and large external reactances [21]. However, power system stabilizers are often used at the machines to reduce oscillations [21]

Chapter 3

Modelling

To analyze how the location of fast frequency resources impacts the system, a 44 bus aggregated model of the Nordic power system was used. The model is named ”Nordic44”, and several versions exist [13]. A description of the model together with assumptions and modifications which have been made, are described in the following sections.

3.1 Area definition

In Nordic 44, the Nordic power system is aggregated into a 44 bus system with 14 areas. The areas do not correspond to the Nordic elspot areas, and in order to use system data from Nord Pool, the areas in Nordic 44 were mapped into elspot areas. The elspot area definition suggested in [12] is also used in this thesis, and is shown in Table 3.1

Elspot area	**Nordic44 area**
NO1	NO1+NO6
NO2 + NO5	NO2+NO3+NO4+NO5
NO3	NO7
NO4	NO8
SE1	SE1
SE2	SE2
SE3	SE3
SE4	SE4
FI	FI1 + FI2

Table 3.1: Mapping of areas in ”Nordic44” into elspot areas

It was mentioned in [12], that load and generation are unevenly modelled in the Nordic44 model. The modification suggested in [12] was used, and buses in SE1 and SE2 were redistributed such that:

- Bus 3100 belongs to SE1

- Bus 3249 belongs to SE2

The single line diagram of the model is shown in in Figure 3.1

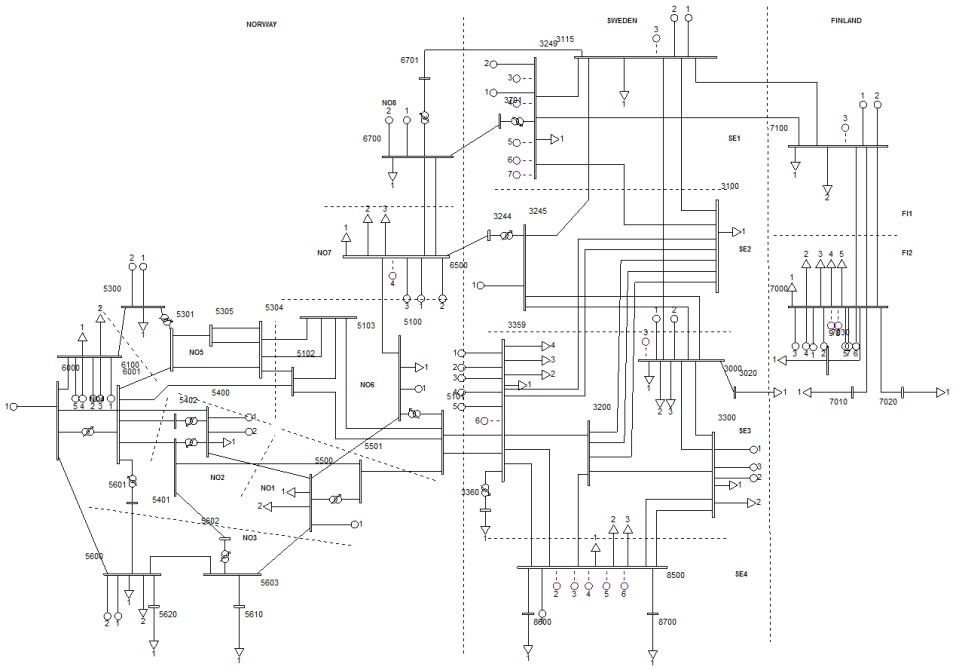

Figure 3.1: Single line diagram of the Nordic 44 model

3.2 Power flow data

The data used for the load flow analysis was based on historical power flow data from Nord Pool [25]. The data from Nord Pool is available at a one hour resolution and the data is given in MWh. Only data for active power load is available, and assumptions on reactive load must be made. Reactive power load was set based on the initial PQ-ratio in the model. When active power of a load was changed, the reactive power of the load was changed such that the PQ-ratio remained the same.

As mentioned in [12], the line impedances in the Norwegian part of the model, might be higher than realistic. This might have been done in the design process of the model in order to get the desired power flow. However, the large impedances in the Norwegian system makes the stability margin low in high export scenarios. To avoid further increase of the production in Norway and simultaneously avoid too large changes in the power flow, losses were accounted for by reducing the load to match the system production. The load reduction was shared equally by each area. Since load and production in set equal before the power flow, system losses are taken by the slack bus. The slack bus is located in SE3,

and the production in this area will therefore increase as compared to the production data given by the Nord Pool data. This might alter the system power flow in some cases. It is however assumed that these changes will have minimal impact on the results.

3.3 HVDC cables

In Nordic44, HVDC cables are modelled as loads. HVDC cables included in this thesis are shown in Table 3.2. Bus data for the HVDC cables in Table 3.2 are based on information in [27] and [12]. All HVDC cables modeled in the system, except FennoSkan, represent power flow to/from external systems. FennoSkan was originally only modelled at bus 3020. Since FennoSkan is an internal HVDC cable, a bus representing the Finnish end of FennoSkan was added to the model. The active power consumption of the HVDC cables were set according to the exchange rates provided from the Nord Pool data.

The reactive power consumption of the HVDC cables depends on HVDC technology and loading of the cable. According to [35], most of the cables used in the model are based on current source converter technology, and are therefore modeled as PQ-nodes in the static power flow. HVDC cables typically consume an amount of reactive power between 50 and 60% of its active power loading [28]. Filters and other equipment may however contribute in reducing the reactive power consumption [28]. For simplicity, reactive power consumption of all HVDC cables were therefore set to 20 percent of the active power loading.

Name	Between areas	Bus number	Capacity [MW]
FennoSkan	SE3 - FI	3020	1300
KontiSkan 1-2	SE3 - DK1	3360	550
Skagerak 1-4	NO - DK1	5610	1700
NorNed	NO - NL	5620	700
VyborgLink	FI-RU	7010	1420
Estlink	FI - ES	7020	1000
BalticCable	SE - DE	8600	600
SwePol	SE - POL	8700	600

Table 3.2: HVDC cables included in the model

3.4 Loads

For power flow simulations in PSS\E, a static power flow simulation is first ran in order to establish initial condition for the dynamic analysis. The case is then converted to a dynamic case. In the steady state power flow analysis, all loads are modeled as constant power loads. For dynamic analysis, loads were converted into constant impedance, constant current and constant power loads (ZIP-loads). From an initial constant power load S_0, the ZIP loads as defined in [17], are given by

$$\begin{aligned} S_I &= \frac{aS_0}{V} \\ S_Y &= \frac{bS_0}{V^2} \\ S_P &= S_0(1-a-b) \end{aligned} \tag{3.1}$$

In (3.1), S_I represents constant current load, S_Y represents constant admittance load, and S_P represents constant power load. S_0 represents the initial constant power load, and the constants a and b represent the share of S_0 which is to be converted into constant current or constant impedance load. V is the voltage at the load when the conversion in made.

In [12], the Nordic44 model was tuned to an outage in Sweden, and ZIP load was set to 10/10/80. The active power ZIP load model used in this thesis was therefore also set to 10/10/80. For the reactive power, values from [24] were used. According to [24], ZIP load parameters of 90/0/10 for reactive power is used by the Swedish TSO, and 90/0/10 for reactive power were therefore also used in this thesis.

3.5 Generators

Rating and maximum power production of the generators in the system is not known. The rating of the parameters `M_Base` and `P_max` was therefore increased proportional to the increase in generated power. The parameter `Q_max` was initially also increased proportionally to the change in generated power. When running the static power flow, some buses did however reach their reactive power limit and were therefore converted from a PV-bus to a PQ-bus by PSS\E.

When modeled as PQ-buses, the voltage at the generator buses is no longer given by its set-point, but rather determined by the power flow solution and the reactive power production. This will alter the power flow solution, and also have an impact on the dynamic simulation results since the static power flow solution is used as initial starting point for the dynamic simulations. To avoid that generator buses becomes PQ buses during static power flow, the change in the reactive power limit of the generators where therefore increased two times the change in the change in active power generation of the generators.

Most of the hydro governors initially had a static droop of 6%. To limit power power output from the generators during power deficit, the static and dynamic droop settings of the hydro governors were doubled in the cases were fast frequency reserves were used. In cases without fast frequency reserves, the droop settings remained unchanged.

3.6 Fault

For frequency stability studies, the outage of a large production unit is critical as this will cause a large power deficit in the system. For comparison reasons, it is desirable to have equal fault size for faults occurring at different locations. To model a generator

outage at a given bus, the production at the bus is rescheduled such that generator 1 has an active power production equal to the chosen size of the fault. The remaining power production is shared equally between the remaining generators. When power production at the generators were changed, the parameters `M_Base`,`P_max` and `Q_max` were increased proportionally to the change in active power production, as described in section 3.5.
The dimensioning fault in the Nordic power system is typically set to 1450 MW, based on the outage of Oskarshamn 3 [19]. Since fault size is kept the same for different fault location, a fault of 1450 MW is not realistic for locations in the rest of the system. The fault size in the simulations were therefore set to 1200 MW.

3.7 Fast frequency reserves

To see how frequency reserve location would affect the power system response to a disturbance, all reserves were located in one area. The impact of generator droop control were limited by increasing generator droop parameters, as mentioned in section 3.5. Since all reserves were located in one area, a total frequency response of 6000 MW/Hz from the FFR reserves were used.

As discussed in section 2.1.3, the power output of fast frequency controlled reserves can be precisely controlled and it can therefore be assumed that the power output from these resources follows the reference power input signal relatively accurately. The PSS\E generator model CBEST is therefore used to represent the fast frequency reserves. CBEST is designed to model the response of a battery with infinite capacity, and the model is therefore well suitable for representing the fast frequency reserves.

A block diagram representation of the CBEST active power control is shown in Figure 3.2. The CBEST takes in a power reference which is given in MW. For the simulations, active power limits are set high in order to avoid saturation and thereby loose information about the dynamic response.

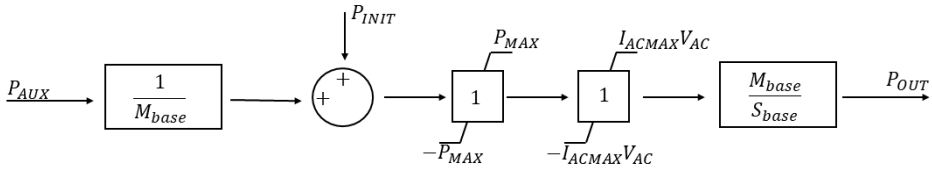

Figure 3.2: Active power control of the PSS\E CBEST model. Based on figure in [16]

Auxiliary power controller

Since CBEST is a generator model, no auxiliary signal model was available in PSS\E. An auxiliary power controller was therefore implemented in python, and simulations were conducted through the PSS\E python API [15]. A proportional controller together with a

filter was implemented in python, and the reference power of the CBEST model, P_{AUX}, where adjusted for each time step.

The auxiliary signal P_{AUX} shown in Figure 3.2 is given in MW, whereas the frequency input signal in PSS\E is given in per unit. To account for differences in unit, the gain of the controller was calculated according to (3.2). Further details of the power control of the CBEST can be found in Appendix B.

$$P_{AUX} = K_p \Delta f_{Hz} = 50 K_p \Delta f_{pu} = K_{fcr} \Delta f_{pu} \tag{3.2}$$

To model an extreme scenario where all the reserves were placed in one area, a frequency response of K_p= 6000 MW/Hz was chosen. K_{fcr} was therefore set to 300 000.

Frequency input filter

A moving averaging filter was used, mainly to introduce a time delay in the output signal. The output signal of a moving averaging filter can be expressed as [11]

$$y[n] = \frac{1}{M} \sum_{k=0}^{M-1} x[n-k] \tag{3.3}$$

were M is the number of samples, y is the output signal, and x is the input signal. The time delay introduced by the moving averaging filter depends on the window size (number of samples) and sampling frequency, T_s. For a step input signal, the moving averaging filter needs the time of its own window length to reach steady state [11]. The filter parameters used for the simulations are given in table 3.3

Parameter	Value
M	10
T_s	0.01

Table 3.3: Filter parameters

3.8 Cases

A high load scenario and a low load scenario was simulated. During initial simulations, damping effects from the FFR were observed. Oscillations in the Nordic system were analyzed through the Nordic44 model in [3], and it was shown that damping were especially low in high load scenarios. Power flow data from 08.01.2015, 05.00-06.00 was therefore used to represent the high load scenario and to demonstrate the effect of damping. According to [25], the lowest total production in the Nordic system in 2015 was on 26.07.2015, 05.00-06.00. Power flow data from 26.07.2015 was therefore used to represent a low load scenario. In the high load scenario, export from Southern Norway to Sweden is high (NO1-SE3), and Finland is importing from Sweden. In the low load case, there is import from Sweden to Southern Norway, and also import from Sweden to Finland. It may be

assumed that differences in inertia and system power flow will be reflected in differences between the two cases, in case those parameters should have a significant impact on the results.

3.9 Simulations

In the simulations, the FFR was located at one location at time, and the response was compared for different fault locations and different FFR locations.

Chapter 4

Simulations and Results

The focus of simulations has been the impact of location and comparison of the frequency response for different cases. The locations are named by their bus number, and details of location may be seen in Figure 3.1. For convenience, a short description of bus location will be given:

- Buses named 3xxx are located in Sweden.
- Buses named 5xxx are located in the south of Norway
- Buses named 7xxx located in Finland.
- Bus 8500 represent SE4 and DK2.
- Bus 6100 is located in Southern Norway

4.1 System response and impact of FFR

To demonstrate the effect of fast response from FFR, the power balance of a hydro generator located in SE2 (bus 3245) and a nuclear generator located in Finland is shown in Figure 4.1. The nuclear power plant at bus 7000 do not participate in primary frequency reserves, and the mechanical power is constant. However, as seen from Figure 4.1, the nuclear power plant do however contribute with inertia, and as kinetic energy is released, the frequency drops. The generator outage occurs at bus 7000, and large rotor swings occurs at the remaining generator.

The impact of FFR is shown in Figure 4.2. It can be seen that the response from FFR is much faster than the mechanical output from the hydro generators. The active power released from the FFR therefore causes less kinetic energy to be released from the synchronous generators, and cause less drop in frequency. For the cases shown in Figure 4.1 and Figure 4.2, generator droop is not reduced and the FFR gain is lower than given in chapter 3.

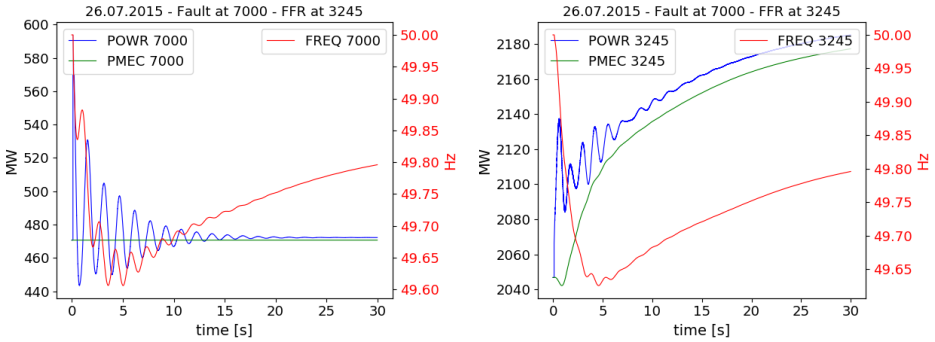

(a) Nuclear generator located at bus 7000 **(b)** Hydro generator located at bus 3245

Figure 4.1: Power and frequency response of different generators

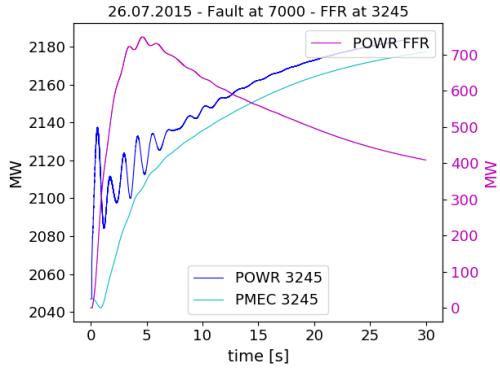

Figure 4.2: Electrical and mechanical power output from a hydro generator together with power output from FFR

4.2 Impact of fault locations on bus frequencies

To see how local frequencies varies without FFR connected, three fault locations in different parts of the grid were chosen, and the variation in frequencies can be seen in Figure 4.3. For all three fault locations, the buses closest to the fault is the most impacted immediately following the fault, whereas buses further away has some delay before the frequency drops. For example when the fault occurs at bus 7000, at t=0.5 seconds the frequency at bus 7000 and bus 7100 drops down to almost 48.85 Hz. The frequency at 6100 is almost unchanged at 0.5 seconds

By comparing the three fault locations, it can also be seen that the fault location has an impact on how much local frequencies differ following a fault. For faults occurring at bus 8500, variations in frequencies are small compared to when the fault occurs at bus 7000 or 5400.

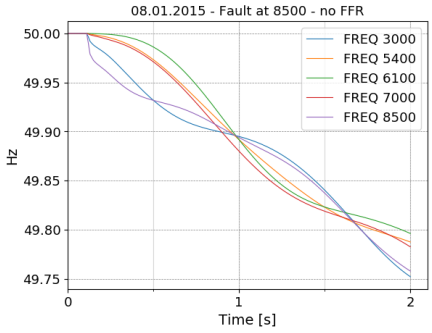

(a) Fault of 1200 MW at bus 8500

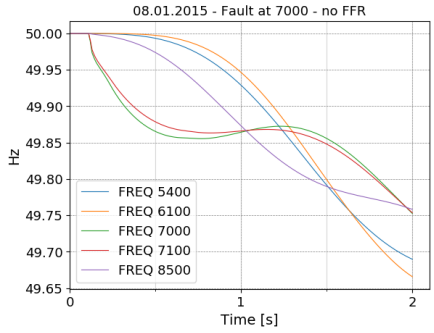

(b) Fault of 1200 MW at bus 7000

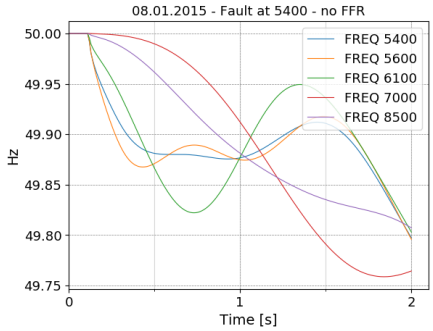

(c) Fault of 1200 MW at bus 5400

Figure 4.3: Frequency response without FFR for different fault locations

4.3 Impact of FFR location on initial frequency drop

Based on the observations made in section 4.2, it may be reasonable to expect that placing FFR close to the fault will cause faster activation of the FFR reserves. To compare different locations of FFR, the frequency at the fault bus was plotted for different locations of FFR and is shown in Figure 4.4. The results shown in Figure 4.4 shows that placing FFR far from the fault causes the frequency to drop lower than when FFR is placed close to the fault. The impact of FFR location do however vary depending on fault location, which could be expected based on observations made in section 4.2.

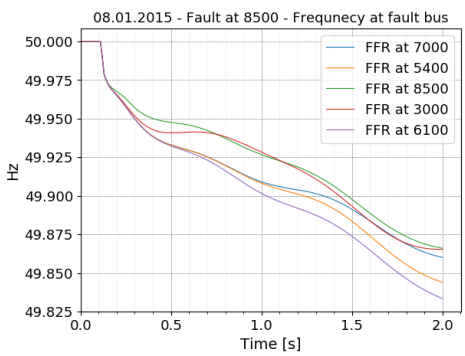

(a) Initial drop in frequency at bus 8500 for different locations of FFR

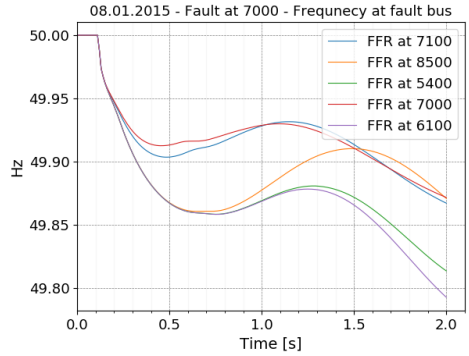

(b) Initial drop in frequency at bus 7000 for different locations of FFR

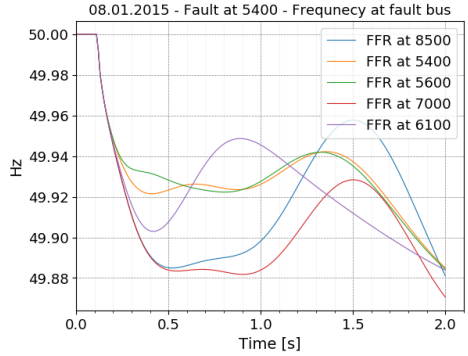

(c) Initial drop in frequency at bus 5400 for different locations of FFR

Figure 4.4: Comparison of initial drop in frequency at the fault bus for different locations of FFR

4.4 Impact of FFR location on frequency nadir

For the three fault locations analyzed in section 4.3, it was shown that placing FFR close to the fault caused a lower initial drop in frequency at the fault bus. Reduced initial drop in frequency indicates that reserves are activated faster, and it may therefore be thought that placing FFR close to the fault would give a higher frequency nadir. Figure 4.5 do however show that the frequency nadir is lowest when FFR are placed close to the fault. If an approximate average of the frequencies in Figure 4.5 is considered, the frequency nadir when FFR are placed on bus 6100 are 49.85 whereas placing the FFR at bus 7000 seems to cause a slightly higher frequency nadir.

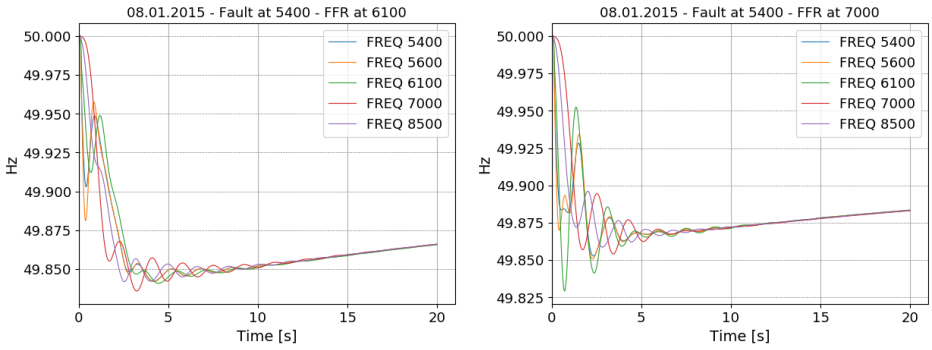

(a) FFR at 6100 (Close to the fault)

(b) FFR at 7000 (Far from the fault)

Figure 4.5: System frequencies when FFR is placed a) close to the fault, and b) far from the fault

To further analyze the impact of location of the frequency nadir, the frequency at the fault bus for different locations of FFR is shown in Figure 4.6. The frequency nadir at the fault bus is compared for cases with different FFR-locations. In all cases, it can be seen that bus 7000 is the location giving the lowest frequency nadir. This indicates that proximity to the fault location do not correspond to the fault location giving the most reduction in frequency nadir.

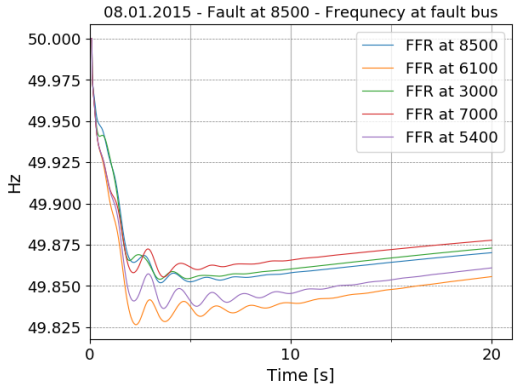

(a) Frequency at bus 8500 for different locations of FFR

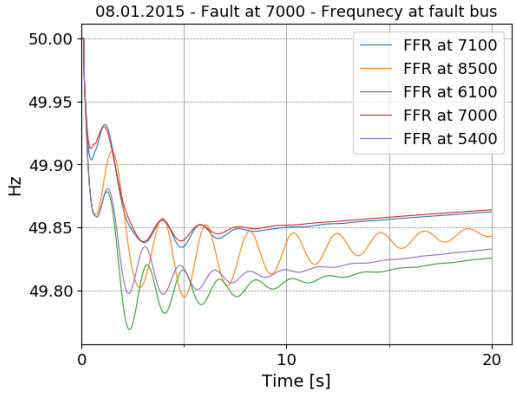

(b) Frequency at bus 7000 for different locations of FFR

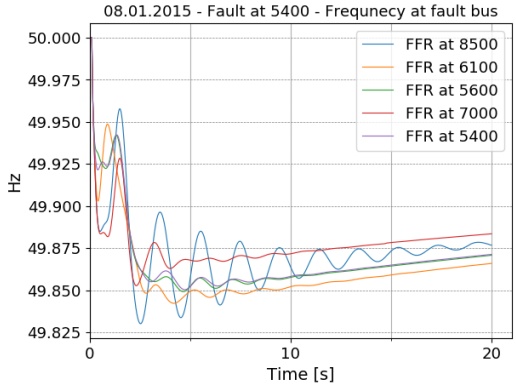

(c) Frequency at bus 5400 for different locations of FFR

Figure 4.6: Comparison of frequency at fault bus for cases with different locations of FFR

Results show that reducing the initial drop in frequency at the fault bus does not necessarily cause an elevation in frequency nadir. This is especially visible for the case where fault occurs at 5400. When the fault occurs at bus 5400, the frequency at bus 7000 was the least impacted (Figure 4.3c), and placing FFR at 7000 had the least impact on the initial drop in frequency for bus 5400 (Figure 4.4c). Placing the FFR at bus 7000 do however give the highest frequency nadir.

By comparing the three fault locations in Figure 4.6, it can be seen that the difference between the highest and the lowest frequency nadir is largest for the case when the fault occurs at bus 7000. This case will therefore be used to further analyze the impact of the FFR location on frequency nadir.

Since the initial drop in frequency at the fault bus is not correlating to the resulting frequency nadir, the active power balance in the system is likely to be different for the three cases. In Figure 4.7 the power output from FFR are shown for a fault at bus 7000. It can be seen that when FFR is placed on bus 6100, the active power output is significantly higher than for the case where where FFR is placed on bus bus 7000. Differences in the system active power balance might be caused by variations in either active power load or active power losses.

Since the load is 80% constant power load, only small load variations are expected. To confirm this, the total system load for the three cases is shown in Figure 4.8. As can be seen, the load variation is small and the lowest load reduction actually occurs when FFR is placed in Finland. This indicates that load variation is not the reason for differences in frequency nadir.

The active power losses of the system is shown in Figure 4.9. It can be seen that in each case, the losses increase. However, by comparing the case with the highest losses (4.9c) and the case with the lowest losses (Figure 4.9b), it can be seen that there is more than 400 MW difference in the peak losses in the two cases. The increase in losses will cause an additional power deficit in the system, and the frequency therefore drops lower in cases when losses are higher.

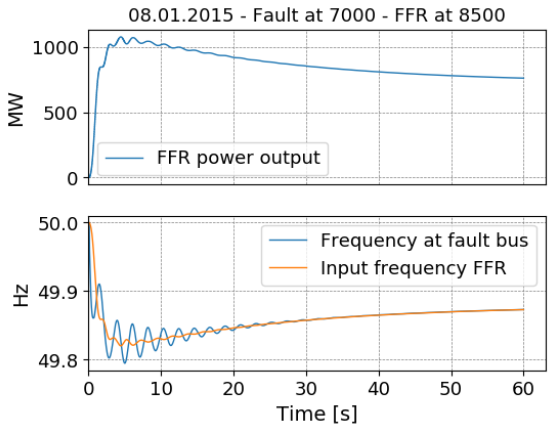

(a) FFR at 8500

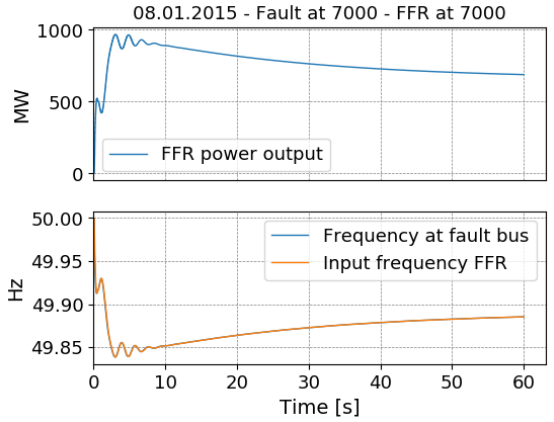

(b) FFR at 7000

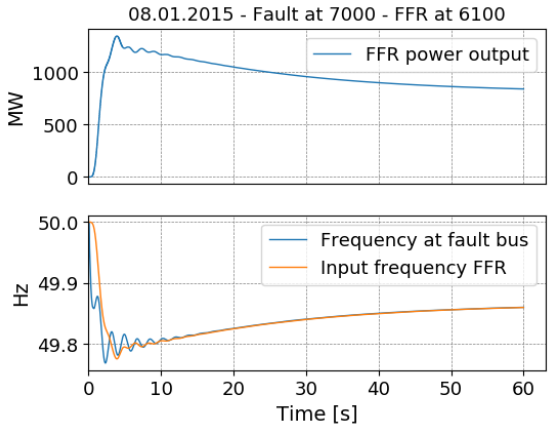

(c) FFR at 6100

Figure 4.7: Power output from FFR at different locations

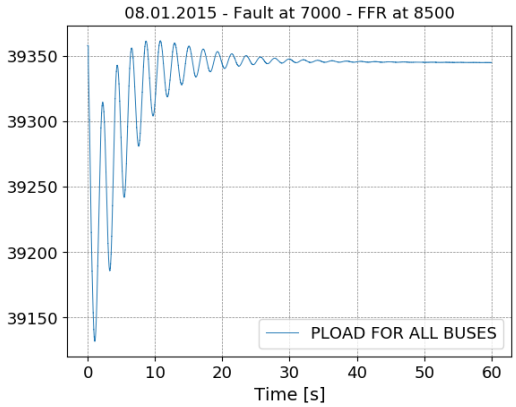

(a) FFR at 8500

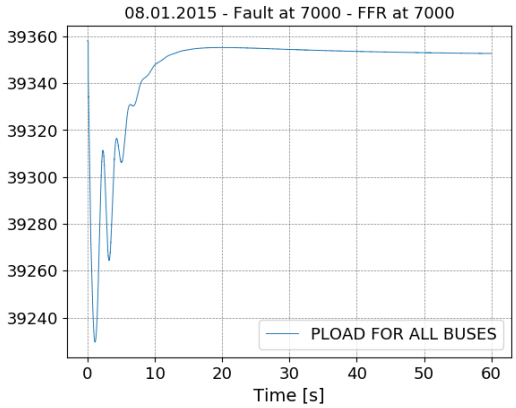

(b) FFR at 7000

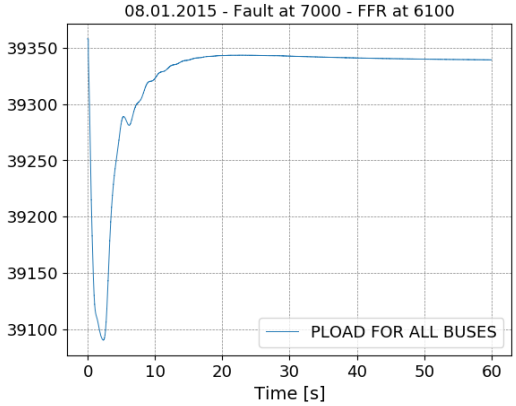

(c) FFR at 6100

Figure 4.8: Total system load for different locations of FFR

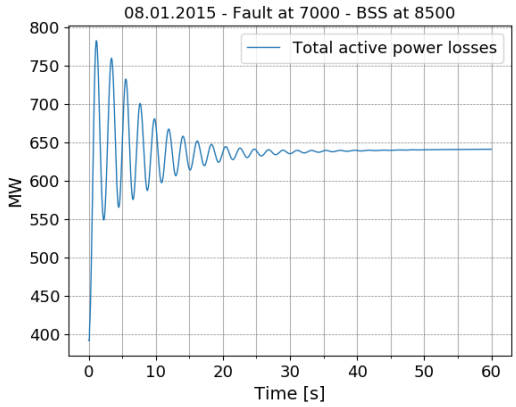

(a) FFR at 8500

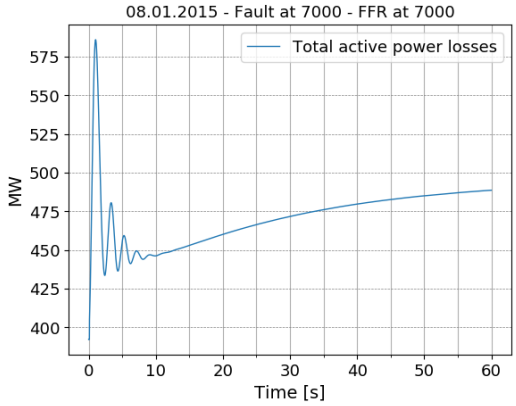

(b) FFR at 7000

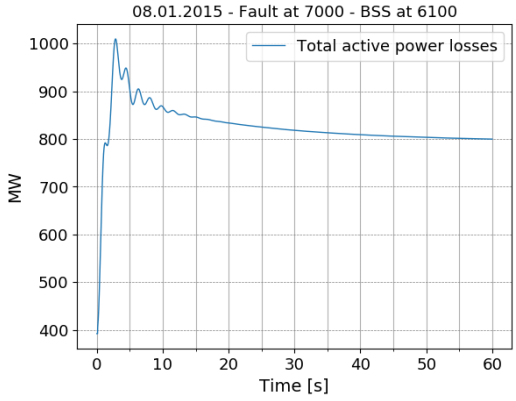

(c) FFR at 6100

Figure 4.9: System losses when fault occurs at bus 7000 and FFR is placed at different locations in the grid

4.5 A low load scenario

The results shown in the previous section were based on a high load scenario. Since inertia and losses will be determined by the power flow scenario, a low load scenario was simulated in order to see if the impact of location would be similar in a low load scenario. The initial drop in frequency for different locations is compared in Figure 4.11, and the frequency nadir for different locations are compared in Figure 4.12.

The results shown in Figure 4.11 and Figure 4.12 shows similar results as in the high load scenario. Placing FFR close to the fault reduces the initial drop in frequency at the fault bus. In the low load scenario, the impact of losses appear to be smaller, and it can be observed from Figure 4.12 that location of FFR has minimal impact on the frequency nadir.

To get an impression of how location of FFR and inertia affects the fault propagation in the system, two cases from two load flow scenarios are compared in Figure 4.10. It can be seen that in the low load scenario, the initial drop in frequency is high, caused by reduced inertia. However, lower inertia seem to accelerate fault propagation which can be seen through increased ROCOF at locations far from the fault. In both scenarios, differences in local frequencies reduces with time.

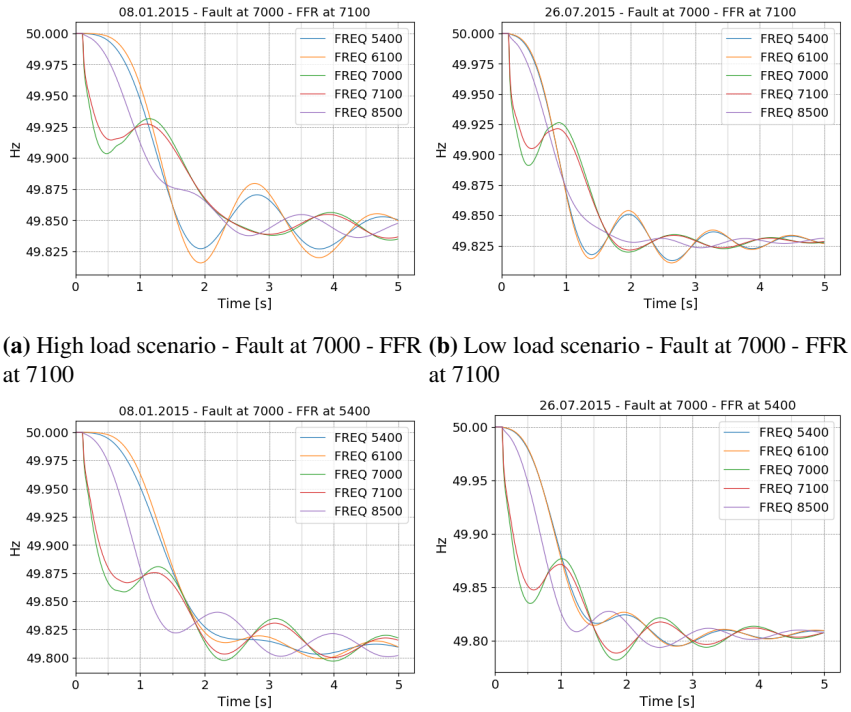

(a) High load scenario - Fault at 7000 - FFR at 7100

(b) Low load scenario - Fault at 7000 - FFR at 7100

(c) High load scenario - Fault at 7000 - FFR at 5400

(d) Low load scenario with fault at 7000 FFR at 5400

Figure 4.10: Comparisons of FFR location in a two scenarios

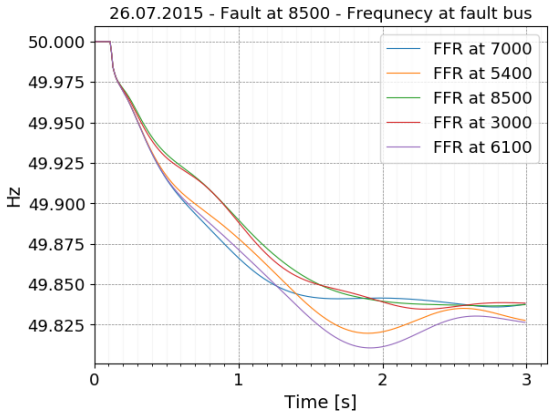

(a) Fault at 8500

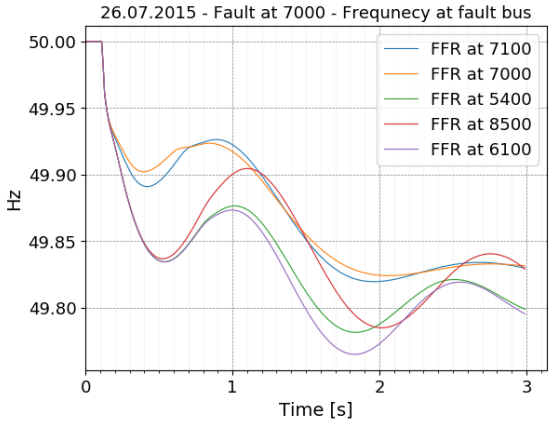

(b) FFR at 7000

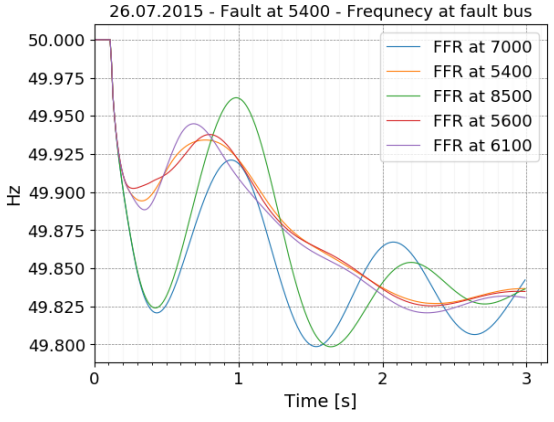

(c) FFR at 5400

Figure 4.11: Comparison of initial drop in frequency for different locations of FFR

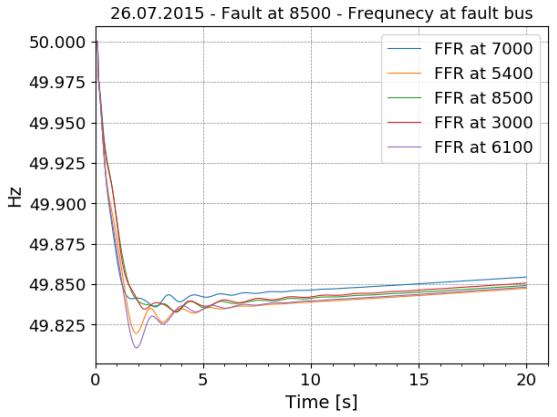

(a) Fault at 8500

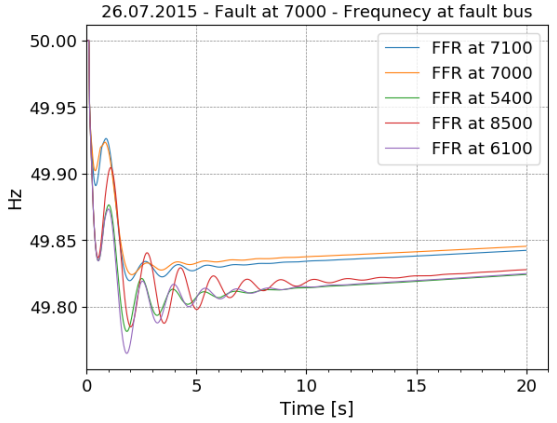

(b) Fault at 7000

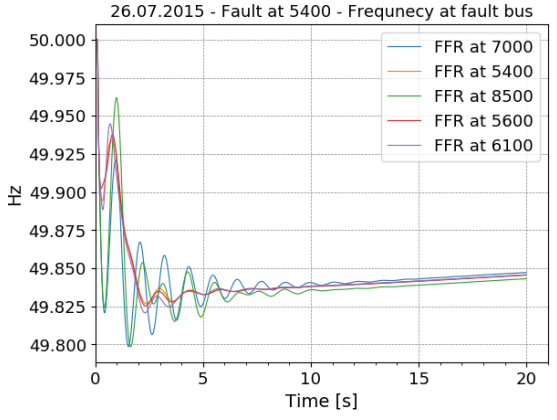

(c) Fault at 5400

Figure 4.12: System losses when fault occurs at bus 5400 and BSS is placed at different locations in the grid

4.6 Power output of FFR

The high load scenario considered in section 4.3 and the low load scenario considered in 4.5 have different levels of inertia. A comparison of the two cases may therefore provide insight in how the FFR location will be impacted for different power flow scenarios and different levels of inertia. The power output from FFR at different locations is plotted for the three fault locations in Figure 4.13. For all three fault locations, it can be seen that when FFR are placed close to the fault, the power output is higher due to larger initial power swings. However, the power back-swing at locations close to the fault causes a delay in power output after the first swing. This effect seems to reduce the initial impact of location.

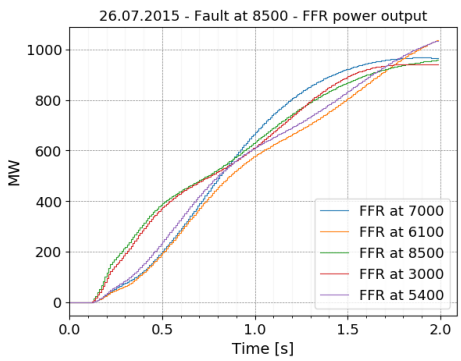

(a) Scenario 26.07.2015 - low load scenario

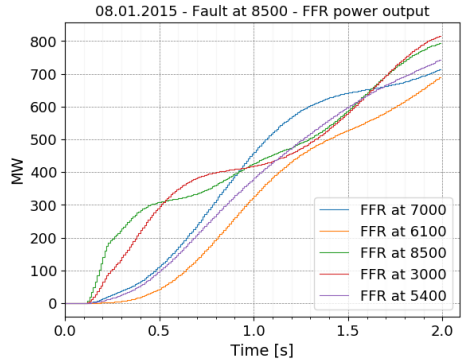

(b) Scenario 08.01.2015 - high load scenario

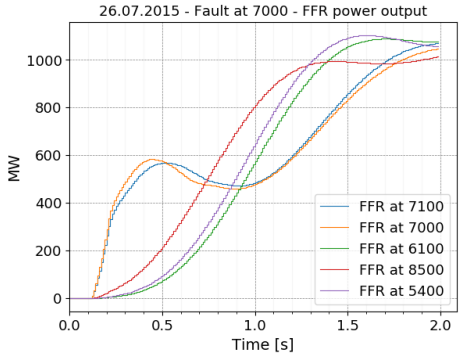

(c) Scenario 26.07.2015 - low load scenario

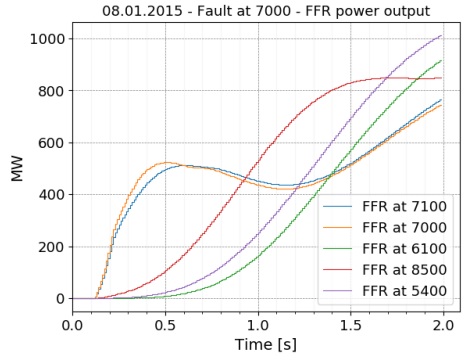

(d) Scenario 08.01.2015 - high load scenario

Figure 4.13: Comparison of FFR power output and location for a high load and a low load scenario

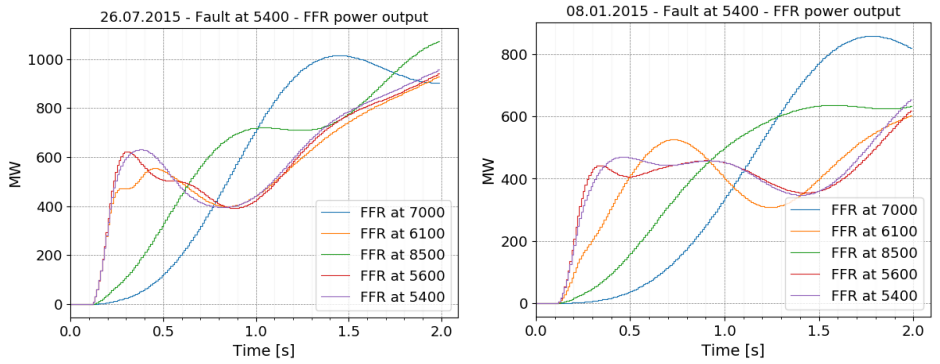

(e) Scenario 26.07.2015 - low load scenario **(f)** Scenario 08.01.2015 - high load scenario

Figure 4.13: Comparison of FFR power output and location for a high load and a low load scenario

4.7 Impact on oscillatory stability

In Figure 4.14, frequencies at different locations in the system are shown for FFR located at 6100 and at 8500.

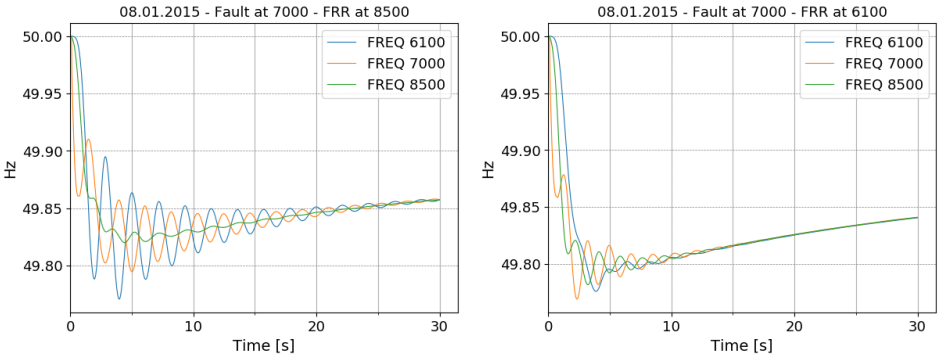

(a) BSS at 8500 **(b)** BSS at 6100

Figure 4.14: FFR effect on damping

It can be seen that the location of FFR has a significant impact on damping in the system. When FFR is placed at bus 6100, the the oscillations between Southern Norway and Finland is significantly reduced, as compared to when the FFR are placed at 8500. This can be explained based on the discussion in section 2.7.2. The power output from the battery is controlled by a proportional controller which takes the bus frequency deviation as input signal. Additionally, the filter sampling window of the controller is short, making the input frequency to the controller in almost perfect phase with the bus frequency. The power

output from the battery will therefore be in phase with the frequency deviation. Since placing the FFR at 6100 will cause the power output from the FFR to be in phase with the frequency deviation at 6100, the power output will contribute in damping the oscillations at 6100. The same damping effect can also be achieved by placing the FFR close to bus 7000, which will be further analyzed in section 4.7.1.

The damping effects by placing the FFR at bus 8500 is however not insignificant. This can be seen by looking at the case with no FFR as shown in Figure 4.15. In case of no FFR, the oscillations between Southern Norway and Finland increases in amplitude, and looses synchronism with each other around t=14 sec.

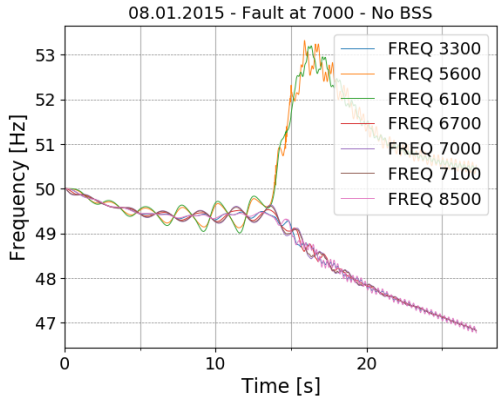

Figure 4.15: Fault at 7000, no FFR

4.7.1 Impact of filter and time delay

As explained in chapter 3.7, a filter is used in the FFR controller. If sampling time is constant, the time delay introduced by the filter depends on the number of samples in the filter. One impact of the filter time delay might be reduced damping. As explained in section 2.7.2, the damping power is in phase with the frequency deviation. A large time delay will shift the power output somewhat out of phase with the actual frequency deviation, and the damping contribution from the FFR is reduced. In Figure 4.16, the frequencies in Finland and Southern Norway is plotted for cases with different sampling windows. It can be seen that an increase from 0.1 second sampling window to 0.3 second sampling window has little impact on the damping. When the sampling window increases to 1.0 seconds, the damping is however significantly reduced.

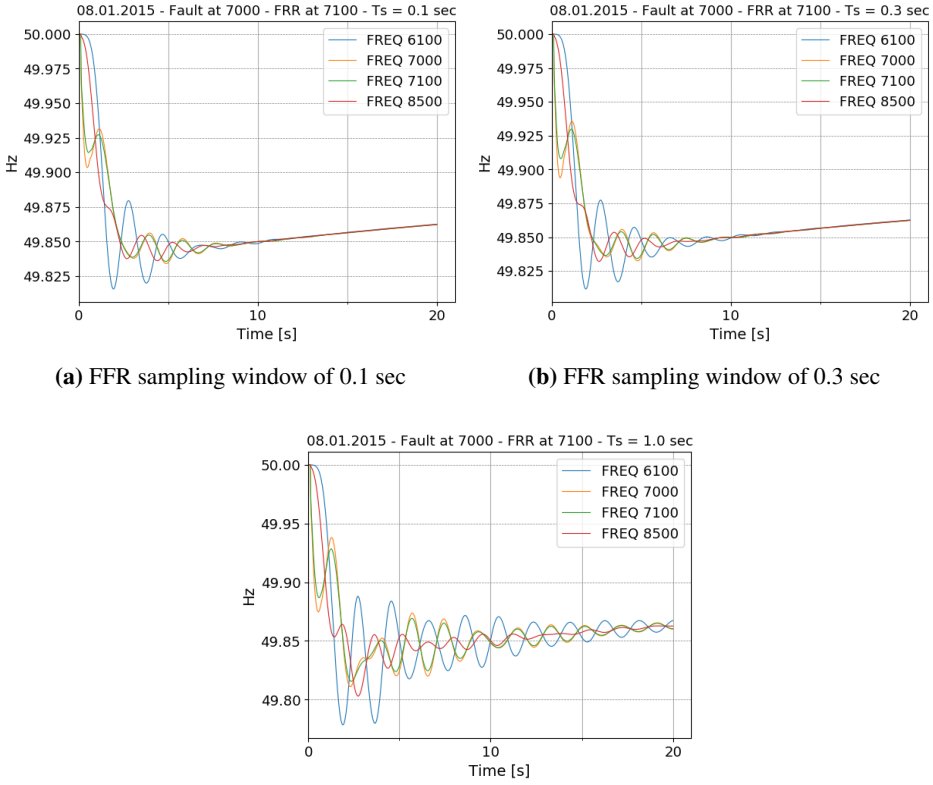

(a) FFR sampling window of 0.1 sec

(b) FFR sampling window of 0.3 sec

(c) FFR sampling window of 1.0 sec

Figure 4.16: Impact of filter sampling on damping

4.7.2 Reserve capacity

As described in section 3.7, the reserve capacity of the FFR was overdimensioned in order to avoid saturation. As reserve capacity is usually limited, it is interesting to look at a case with limited reserves. This is shown in Figure 4.17, and it can be seen that reserve capacity has impact on both frequency nadir and the contribution of damping from the FFR.

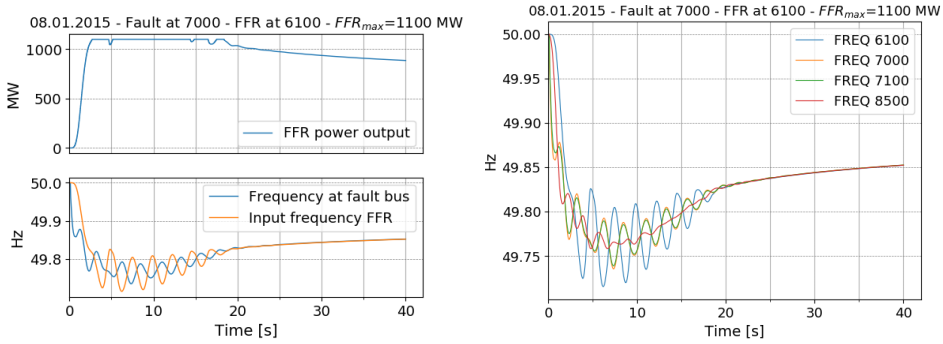

(a) BSS power output

(b) System frequencies with BSS at 6100

Figure 4.17: Effect of losses when frequency reserves are limited

Chapter 5

Discussion

The extreme response achieved through concentrating the FFR reserves in only one area clearly shows that location will affect the system response, stability and reserve requirements.

Impact of electrical distance

The impact of electrical distance is clearly seen in the model. When a fault occurs in Finland or Southern Norway, there are significant differences in variations of local frequencies. When the fault occurs in Southern Sweden, less variations in local frequencies are seen. The results indicate that in Southern Norway and Finland, the share of synchronizing power coefficient for generators close to each other is large. In southern Sweden, the share of synchronizing power coefficient seem to be more equally distributed, resulting in less variations of local frequencies immediately following a fault.

The impact of electrical distance resulted in large power swings at locations close to the fault when the fault occurred in Southern Norway or Finland. The immediate drop in frequency at fault locations in Southern Norway and Finland therefore caused a higher initial power output from the FFR reserves when the reserves were placed close to the fault (Figure 4.13). When reserves were placed close to the fault, the initial high power output also contributed in damping the initial swing at the fault location (Figure 4.4 and Figure 4.11).

Impact of location on Frequency nadir

Despite large differences in power output immediately following a fault, it was shown in Figure 4.12 that location of FFR had little impact on the frequency nadir. The power output from FFR close to the fault is quickly activated due to the initial power swing. However, as the fault propagates, a larger share of the load is taken by the rest of the system, and differences in local frequencies reduces. Since increased variations in local frequencies and lower inertia will contribute in accelerating the fault propagation, similar results may be expected for other scenarios as well.

Impacts on oscillatory stability

As explained in section 4.7, accurate control of FFR power output increases the damping power. By placing FFR at locations where the frequency tends to participate in low frequency oscillations, the power output from the FFR will contribute in dampen these oscillations. In the case '08.01.2015', low frequency oscillations between Southern Norway and Finland is poorly dampened, and disturbances in any of the two areas will excite oscillatory behaviour between Southern Norway and Finland. It was shown in section 4.7 that placing FFR in an area were the amplitude of oscillations were high, contributed in significant damping of system oscillations.

As mentioned in section 2.1.2, low frequency oscillations have a significant impact on the frequency quality and the required FCR-N reserves. The results shown in section 4.7 indicate that placing the reserves appropriately may reduce oscillations in the system. System stability and frequency quality may thereby be enhanced.

FFR was however modeled with a sampling window of 0.1 seconds. As shown in Figure 4.16, increasing the sampling window to 1.0 seconds causes reduced damping. Optimal damping effect will also be lost if sufficient reserves are not available, as is illustrated in Figure 4.17.

Impact of losses

Losses is currently not considered when frequency reserves are procured by the TSOs [29]. Although the results showed a significant impact of losses, the concentrated placement of the reserves are not realistic, and smoothing effects in cases with more distributed reserve allocation will probably make the impact of losses less significant. However, the case "08.01.2015" clearly illustrates that in cases with high initial losses, the location of FFR might significantly increasing the losses. In the case "08.01.2015", import to Finland was high, whereas Southern Norway had high export. The case shows that placing the reserves in import areas such as Finland may cause a reduction in system losses. Similarly, placing reserves in export areas such as Southern Norway is likely to cause an increase in system losses, and thereby increased need for reserves.

Impact of location and power output

The results indicated that if a fault occurs in areas which is weakly connected to the rest of the system (high share of synchronizing power coefficient), large initial frequency excursions will occur close to the fault. Placing fast reserves in these areas will therefore cause fast activation, and reduce the impact of the fault. However, the results presented in chapter 4, indicate that activation will only have local impacts immediately following the fault, and if all generators remain in synchronism, location will not impact the system frequency nadir.

Assumptions impacting the results

The load model is likely to have an impact on the results. The active power was set to 85 $\%$ constant power load, and with more voltage dependent load, other effects due to variations in load might occur. For reactive power, the share of constant power load is only 10%, whereas 90% of the reactive power is constant impedance load. With a higher share of constant reactive power load, issues related to voltage stability may occur.

Frequency measurements in PSS\E is based on the derivative of bus voltage angle. There might therefore be cases where bus frequency in PSS\E do not correspond to the rate of change of rotor angles [4]. This issue is however neglected.

Chapter 6

Conclusion and Future Work

By comparing different locations of FFR, it has been shown that location has little impact on the frequency nadir caused by a sudden power deficit. The effect of electrical distance to the fault had great impact on the initial frequency for certain fault locations. At locations with high share of synchronizing power coefficient to the fault bus, the initial drop in frequency will be reduced if FFR is located close to these buses. Large initial differences did however seem to balance out during inertial response of the generators, and location therefore had little impact on the frequency nadir.

Location do however seem to have great impact on damping of low frequency oscillations. In scenarios with poorly dampened oscillations, the damping effect of FFR is beneficial for system operation, and should be taken advantage of by the TSOs when locating reserves.

FFR was however modeled with a sampling window of 0.1 seconds. Increasing the sampling window also increases the delay, and the results showed that damping effect was reduced when delay increased. The FFR product considered by the Norwegian TSO has a maximum activation time of 2 seconds [29]. Such a product might therefore not contribute considerably to damping. Stricter activation requirements might however limit market participants. Further studies on the impact of time delay and optimal limits for activation time with respect to damping will therefore be an interesting topic to include in future work.

Due to the high share of constant power load used in the simulations, load variations had little impact on the results. Higher voltage dependency of loads might cause local impacts which should be considered in future work. The impact of distribution of inertia is also an interesting topic which has not been considered in the simulations.

Bibliography

[1] P.M. Anderson and A. A. Fouad. *Power system control and stability*. eng. Piscataway, N.J, 2003.

[2] Sunniva Bjelland. "Power System Frequency Control and Security of Supply (Unpublished)". 2018.

[3] Knut Bjørsvik. *A Scheme for Creating an Small-Signal On-line Dynamic Security Assessment Tool - Using PSS/E and PacDyn*. eng. 2016. URL: http://hdl.handle.net/11250/2400486.

[4] D. Doheny and M. Conlon. "Investigation into the local nature of rate of change of frequency in electrical power systems". In: *2017 52nd International Universities Power Engineering Conference (UPEC)*. Aug. 2017, pp. 1–6. DOI: 10.1109/UPEC.2017.8231982.

[5] EirGrid and SONI. *Consultation on DS3 System Services Protocol Document*. 2018.

[6] ENTSOE. *Appendix 1 of System Operation Agreement*. 2018.

[7] ENTSO-E. *ELECTRICITY BALANCING IN EUROPE*. 2018.

[8] ENTSO-E. *Frequency Containment Reserves (FCR)*. 2019. URL: https://www.entsoe.eu/network_codes/eb/fcr/ (visited on 02/11/2019).

[9] ENTSO-E. *Nordic Balancing Philosophy*. 2016.

[10] Fingrid. *Frequency quality analysis 2017*. 2018.

[11] S. Golestan et al. "Moving Average Filter Based Phase-Locked Loops: Performance Analysis and Design Guidelines". In: *IEEE Transactions on Power Electronics* 29.6 (June 2014), pp. 2750–2763. ISSN: 0885-8993. DOI: 10.1109/TPEL.2013.2273461.

[12] Silje Mork Hamre. *Inertia and FCR in the Present and Future Nordic Power System - Inertia Compensation*. eng. 2015. URL: http://hdl.handle.net/11250/2368231.

[13] Sigurd Hofsmo Jakobsen and Lester Kalemba. *The Nordic 44 test network*. 2018.

[14] IEA International Energy Agency. *Status of Power System Transformation 2017*. 2017.

[15] Siemens Power Technologies International. *PSS\E 33.5 APPLICATION PROGRAM INTERFACE (API)*. 2013.

[16] Siemens Power Technologies International. *PSS\E 33.5 MODEL LIBRARY*. 2013.

[17] Siemens Power Technologies International. *PSS\E 33.5 Program Operation Manual*. 2013.

[18] Affärsverket Svenska kraftnät et al. *Cooperation Agreement Nordic balancing cooperation*. 2018.

[19] Mikko Kuivaniemi, Niklas Modig, and Robert Eriksson. *FCR-D design of requirements*. ENTSO-E, 2017.

[20] P Kundur. *Power system stability and control*. eng. The EPRI power system engineering series. New York: McGraw-Hill, 1994. ISBN: 9780070359581.

[21] T. A Lipo. *Analysis of Synchronous Machines, Second Edition*. eng. 2nd ed. CRC Press Inc, 2012. ISBN: 1439880670.

[22] Jan Machowski. *Power system dynamics : stability and control*. eng. 2nd ed. Chichester: Wiley, 2008. ISBN: 9780470725580.

[23] Erik Ørum et al. *Frequency Quality, phase 2*. Project Report - Version 1.2. Entsoe, 2017.

[24] Adriel Perez Tellez. "Modelling aggregate loads in power systems". eng. PhD thesis. 2017.

[25] Nord Pool. *Historical Market Data*. 2018. URL: https://www.nordpoolgroup.com/historical-market-data/.

[26] Ciaran Roberts. *Review of International Grid Codes*. 2018.

[27] Espen Hafstad Solvang. *Dynamic Simulations of Simultaneous HVDC Contingencies in the Nordic Power System Considering System Integrity Protection Schemes*. eng. 2018. URL: http://hdl.handle.net/11250/2561568.

[28] Vijay K. Sood. "30 - HVDC Transmission". In: *Power Electronics Handbook (Second Edition)*. Ed. by Muhammad H. Rashid. Second Edition. Engineering. Burlington: Academic Press, 2007, pp. 769–795. ISBN: 978-0-12-088479-7. DOI: https://doi.org/10.1016/B978-012088479-7/50048-1. URL: http://www.sciencedirect.com/science/article/pii/B9780120884797500481.

[29] Statnett. *Roller i balansemarkedene og vilkår for aggregerte bud*. Norwegian. 2018.

[30] Statnett. *Tall og data fra kraftsystemet*. 2018. URL: https://www.statnett.no/for-aktorer-i-kraftbransjen/tall-og-data-fra-kraftsystemet/#nordisk-kraftflyt.

[31] Statnett et al. *Challenges and Opportunities for the Nordic Power System*. 2016.

[32] Statnett et al. *The Way forward - Solutions for a changing Nordic power system*. 2018.

[33] Kjetil Uhlen and Olav Bjarte Fosso. *Power system operation and Frequency control (lecture notes)*.

[34] Andreas Ulbig, Theodor S. Borsche, and Göran Andersson. "Analyzing Rotational Inertia, Grid Topology and their Role for Power System Stability". In: *IFAC-PapersOnLine* 48.30 (2015). 9th IFAC Symposium on Control of Power and Energy Systems CPES 2015, pp. 541–547. ISSN: 2405-8963. DOI: https://doi.org/10.1016/j.ifacol.2015.12.436. URL: http://www.sciencedirect.com/science/article/pii/S2405896315030785.

[35] Til Kristian Vrana et al. *Impact of present and future HVDC links on the nordic power grid*. eng. 2017. URL: http://hdl.handle.net/11250/2450834.

Appendix A

Dynamic properties used for the CBEST model is shown in Table 6.1. Parameter names corresponds to the dynamic parameters given in [16]

Parameter	**Value**
PMAX	2
OutEff (>= 1) Output Efficiency	1.1
InpEff (<= 1) Input Efficiency	0.9
IACMAX	2.0
KAVR	1.0
T1	0
T2	0
T3	0.05
T4	0
VMAX, AVR Speed Limit	10
VMIN, AVR Speed Limit	-10
Droop	0.005

Table 6.1: Dynamic parameters of the CBEST model

Appendix B

The parameter Kd in the code was included for the possibility to use a derivative controller. A derivative controller was not used and Kd was set to zero for all cases.

```
# Disconnect generators and run for rest of simulation time
psspy.dist_machine_trip(bus_fault,r'%s' %m_id_fault)  #Disconnects gener
f0=0

for x in range(10,steps):
    ierr, busfreq = psspy.chnval(1) #get bus frequency
    # ================ FILTER ================================
    temp = window[1:len(window)+1] # Storing the old window, except the
    window[:-1] = temp
    window[-1] = busfreq
    fltrd_freq = sum(window)/wsize
    freq_filtered[x] = fltrd_freq
    time_filter[x] = t
=========================================================
    #ROCOF
    f1=fltrd_freq
    ROCOF=(f0-f1)/timestep
    f0=f1
    p_rocof=Kd*ROCOF
    #Change BSS power reference and run simulation for one timestep
    p_freq=k_fcr*fltrd_freq #MW
    p_ref_bess = p_rocof +p_freq #if rocof is activated (if Kd !=0 )
    ierr = psspy.change_plmod_var(bus_BS,'BS', 'CBEST', 1, p_ref_bess)
    t = t+timestep
    psspy.run(0, t,1,1,0) #run until t sec
```

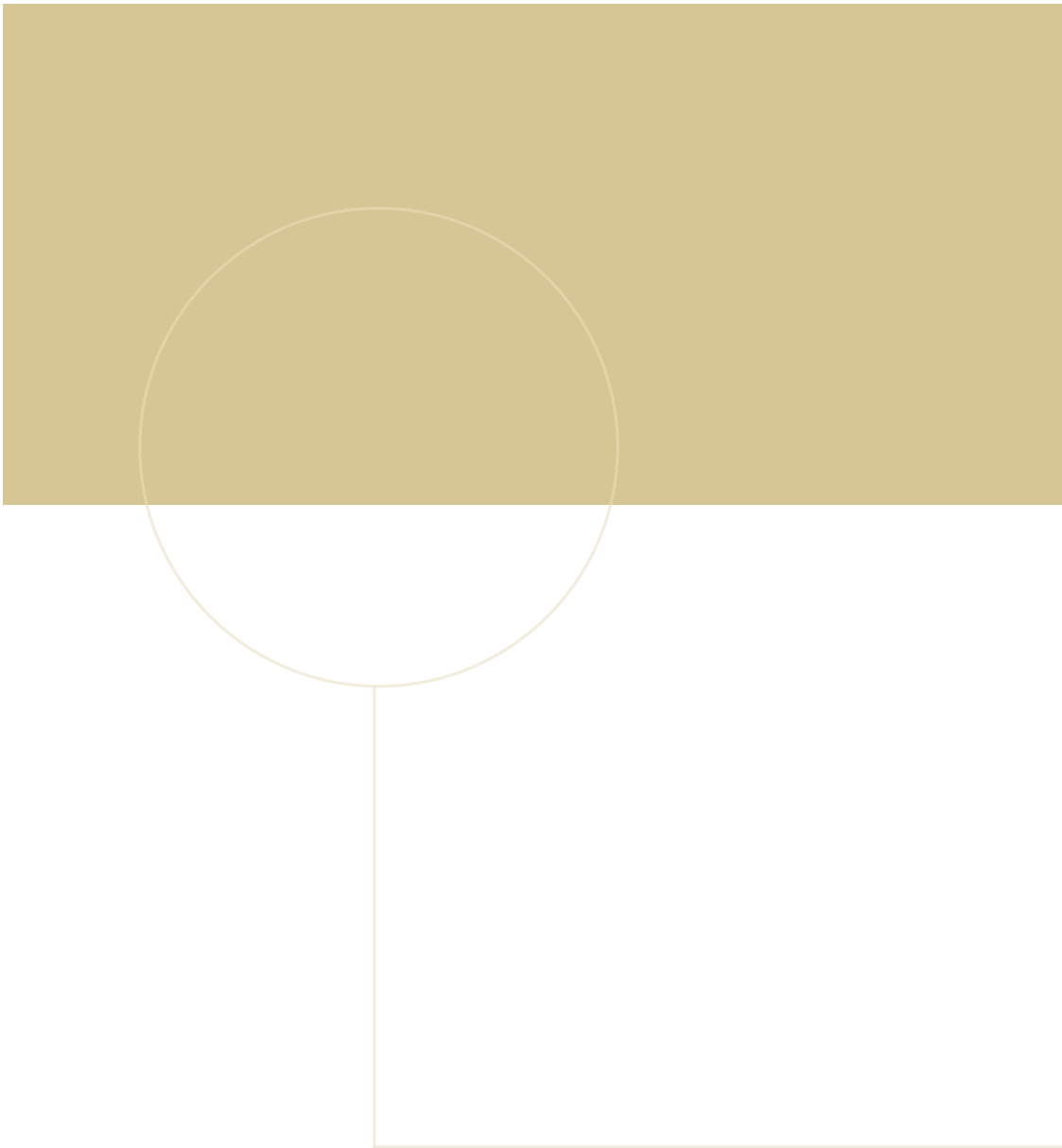

NTNU
Norwegian University of
Science and Technology